JOURNAL OF GEOPHYSICAL RESEARCH, VOL. 115, C06006, doi:10.1029/2009JC005821, 2010

Isopycnal diffusivities in the Antarctic Circumpolar Current inferred from Lagrangian floats in an eddying model

A. Griesel,[1] S. T. Gille,[1] J. Sprintall,[1] J. L. McClean,[1] J. H. LaCasce,[2] and M. E. Maltrud[3]

Received 23 September 2009; revised 9 December 2009; accepted 5 January 2010; published 10 June 2010.

[1] Lagrangian subsurface isopycnal eddy diffusivities are calculated from numerical floats released in several regions of the Antarctic Circumpolar Current (ACC) of the 0.1° Parallel Ocean Program. Lagrangian diffusivities are horizontally highly variable with no consistent latitudinal dependence. Elevated values are found in some areas in the core of the ACC, near topographic features, and close to the Brazil-Malvinas Confluence Zone and Agulhas Retroflection. Cross-stream eddy diffusivities are depth invariant in the model ACC. An increase of Lagrangian eddy length scales with depth is masked by the strong decrease with depth of eddy velocities. The cross-stream diffusivities average 750 ± 250 m^2 s^{-1} around the Polar Frontal Zone. The results imply that parameterizations that (only) use eddy kinetic energy to parameterize the diffusivities are incomplete. We suggest that dominant correlations of Lagrangian eddy diffusivities with eddy kinetic energy found in previous studies may have been due to the use of too short time lags in the integration of the velocity autocovariance used to infer the diffusivities. We find evidence that strong mean flow inhibits cross-stream mixing within the ACC, but there are also areas where cross-stream diffusivities are large in spite of strong mean flows, for example, in regions close to topographic obstacles such as the Kerguelen Plateau.

Citation: Griesel, A., S. T. Gille, J. Sprintall, J. L. McClean, J. H. LaCasce, and M. E. Maltrud (2010), Isopycnal diffusivities in the Antarctic Circumpolar Current inferred from Lagrangian floats in an eddying model, *J. Geophys. Res.*, *115*, C06006, doi:10.1029/2009JC005821.

1. Introduction

[2] Mixing generated by mesoscale eddies is believed to play an important role in the transfer of water masses and tracers across the Antarctic Circumpolar Current (ACC) [*Johnson and Bryden*, 1989; *Marshall et al.*, 1993; *Döös and Webb*, 1994; *Speer et al.*, 2000; *Bryden and Cunningham*, 2003; *Marshall and Radko*, 2003]. This eddy "mixing" is thought to be highly variable in time and space [*Visbeck et al.*, 1997; *Treguier et al.*, 1997; *Stammer*, 1998]. In coarse resolution ocean models, an eddy diffusivity parameterization is commonly used to incorporate the effects of eddies [*Gent and McWilliams*, 1990; *Griffies*, 1998]. However, it remains unclear whether eddy diffusion represents an appropriate parameterization. In addition, coarse resolution models are sensitive to the magnitude, and the horizontal and vertical distributions of the eddy mixing coefficients [*Danabasoglu and Marshall*, 2007].

[3] Lagrangian floats provide a way to test the applicability of the eddy diffusion model (see *LaCasce* [2008] for an overview). *Taylor* [1921] showed how Lagrangian particles in isotropic and homogeneous turbulence spread diffusively, with a constant diffusivity calculated from the integral of the velocity autocorrelation. *Davis* [1987, 1991] refined the theoretical framework to allow both the mean flow and diffusivity to be spatially variable, and to allow the theory to be applied to ocean float data. In an ocean with inhomogeneous, strong mean flows and with an eddy field of varying horizontal scale, one challenge is to find the asymptotic behavior of the velocity autocorrelation, which requires sufficiently long time lags [e.g., *Bauer et al.*, 1998; *Veneziani et al.*, 2004; *Davis*, 2005]. A second challenge arises because of the presence of vortices or meanders that lead to oscillations in the autocovariances. The oscillations cause regimes of primarily subdiffusive behavior at intermediate time lags [*Berloff and McWilliams*, 2002a, 2002b; *Veneziani et al.*, 2005b]. Questions remain as to whether this is a transient behavior, and whether the diffusive limit can still be reached after long enough time lags.

[4] Diffusivities are hypothesized to be connected to the kinetic energy of the mixing eddies. For example, both *Keffer and Holloway* [1988] and *Stammer* [1998] used altimetric sea surface height variability to estimate surface eddy diffusivities. Diffusivities inferred from Lagrangian floats are also often highly correlated with eddy kinetic energy [*Krauss and Böning*, 1987; *Lumpkin et al.*, 2001; *Zhurbas and Oh*, 2004; *Sallée et al.*, 2008]. A recent study found

[1] Scripps Institution of Oceanography, University of California, San Diego, La Jolla, California, USA.
[2] Meteorology and Oceanography Section, Department of Geosciences, University of Oslo, Oslo, Norway.
[3] Los Alamos National Laboratory, Los Alamos, New Mexico, USA.

0148-0227/10/2009JC005821

variations in eddy stirring and mixing rates using finite time Lyapunov exponents to be closely related to variations in eddy kinetic energy [*Waugh and Abraham*, 2008]. While eddy activity is enhanced in regions with strong currents such as in the ACC, these strong currents can also act as mixing barriers [*Bower et al.*, 1985], leading to small effective eddy diffusivities [e.g., *Marshall et al.*, 2006; A. C. Naveira Garabato et al., Eddy-induced mixing in the Southern Ocean, submitted to *Journal of Physical Oceanography*, 2009]. At any given geographic location, the magnitude of the diffusivity depends on the relative importance of these two factors [*Shuckburgh et al.*, 2009a, 2009b]. For the near-surface Southern Ocean, *Sallée et al.* [2008] found a local maximum of Lagrangian diffusivities in the core of the ACC that, at some longitudes, seemed to be correlated with enhanced eddy kinetic energy. In contrast, using a different method, *Marshall et al.* [2006] obtained effective diffusivities at the surface about half as large as *Sallée et al.* [2008], with a minimum of diffusivities in the core of the ACC jet. This implied that the ACC jet acted as a mixing barrier in the along-streamline average.

[5] Inferences of depth dependence of eddy diffusivities often rely on whether eddy kinetic energy or the eddy length scales are used to determine the diffusivity. If eddy diffusivity scales like the eddy heat flux or like eddy kinetic energy, a decrease with depth might be expected [*Phillips and Rintoul*, 2000]. Such a decrease was found for the Southern Ocean by *Ferreira et al.* [2005], who fitted eddy stresses in a coarse model to hydrographic data; by *Olbers and Visbeck* [2005] from a simple inverse approach using hydrographic and wind stress data; and by *Eden* [2006] and *Griesel et al.* [2009] using methods based on flux-gradient relationships. Conversely, critical layer theory predicts that the diffusivity should have a maximum at the depth where the speed of the mean flow is comparable to the phase speed of Rossby waves [*Green*, 1970; *Killworth*, 1997; *Smith and Marshall*, 2009]. Critical layer theory suggests that at the ocean surface, mixing efficiency is reduced since the strong current carries the eddies downstream so quickly that they do not have much time to mix. However, at a depth of about 1–2 km, the eddies propagate at the same speed as the mean flow, and eddies are therefore able to mix fluid elements. This leads to higher mixing rates at depth. Indeed, enhanced diffusivities at depth in the ACC have been diagnosed by *Treguier* [1999], *Cerovecki et al.* [2009], *Smith and Marshall* [2009], and *Abernathy et al.* [2009] in models of varying complexity, using either flux-gradient relationships or the *Nakamura* [1996] method that evaluates the stretching and folding of the contours of a passive tracer as it is mixed and stirred by the eddies. At present, virtually no reliable observations exist in the Southern Ocean to validate the depth dependence of the model eddy diffusion coefficients.

[6] In this paper, we estimate isopycnal eddy diffusivities from the dispersion of Lagrangian numerical floats released in core regions of the ACC in a fine resolution configuration of the Parallel Ocean Program (POP). Our intent is first to explore whether a diffusive limit can be reached after long enough time lags of the velocity autocorrelations. This effort will demonstrate that the theoretical framework of *Taylor* [1921] and *Davis* [1987, 1991] is appropriate for determining representative diffusivities if appropriate means are subtracted. Using these eddy diffusivities, our second goal is to determine the magnitude, and the horizontal and vertical distributions of the Lagrangian diffusivities in the Southern Ocean. Our study will show elevated diffusivities in the core of the ACC and in eddy-rich areas such as the Malvinas Confluence and the Agulhas Retroflection. However, we find the cross-stream eddy diffusivities to have no significant depth dependence. Finally, our third objective is to examine the relationship of the diffusivities to the eddy kinetic energy and strength of the mean flow. Our results suggest that parameterizations that only use eddy kinetic energy to parameterize the diffusivities are misleading. We also find that Lagrangian diffusivities are not consistently reduced in regions with strong mean flow.

[7] This paper is organized as follows. In section 2 we will introduce the model and outline the float deployments and trajectories. Section 3 discusses the method used to compute the Lagrangian diffusivities. Section 4 examines whether a diffusive limit is reached, and what role the mean flow, streamline projections and rotational components of the eddies play. Section 5 shows the horizontal and vertical distributions of the binned Lagrangian diffusivities and discusses their relationship to the eddy kinetic energy and mean flow. Section 6 presents the conclusions.

2. Model Description

[8] We use the 1/10° global POP model, described in detail by *Maltrud and McClean* [2005] and used by *Griesel et al.* [2009] to assess eddy heat flux parameterization in the Southern Ocean. This simulation has one of the highest horizontal resolutions used to date in global ocean modeling. Its Mercator grid results in a horizontal resolution between 4 and 9 km in the Southern Ocean, which is sufficient to resolve the first baroclinic Rossby radius north of about 50°S. Vertical resolution is between 10 m at the surface and 250 m at depth. The model was spun up for 14 years (1979–1993), and then run with realistic forcing from 1994 to 2003 (see *Maltrud and McClean* [2005] for details). Lagrangian eddy scales calculated from surface drifters in the model have been shown to be comparable to observations in the North Atlantic [*McClean et al.*, 2002].

[9] Horizontal diffusion is biharmonic for tracers and momentum, as discussed by *Maltrud and McClean* [2005] and by *Griesel et al.* [2009]. For vertical mixing in the model, the K profile parameterization of *Large et al.* [1994] is used, with background mixing coefficients ranging from 0.1×10^{-4} m^{2}s^{-1} near the surface to 1×10^{-4} m^{2}s^{-1} at depth. The subgrid scale parameterizations, as well as spurious numerical diffusion originating from the tracer advection discretization can all potentially introduce diapycnal velocities through the *Veronis* [1975] effect, and thus may contribute to the Lagrangian motions of particles in the model. For the purpose of this paper we assume this effect to be negligible.

2.1. Float Trajectories

[10] Our analysis focuses on numerical floats deployed in 4 patches of 80 floats at each of three depths, initially at 300 m, 800 m, and 1500 m (Figure 1). The deployment patches were sited within the core of the ACC around 55°S. In each patch, floats were deployed on a grid with quarter degree spacing in latitude and longitude. This spacing was

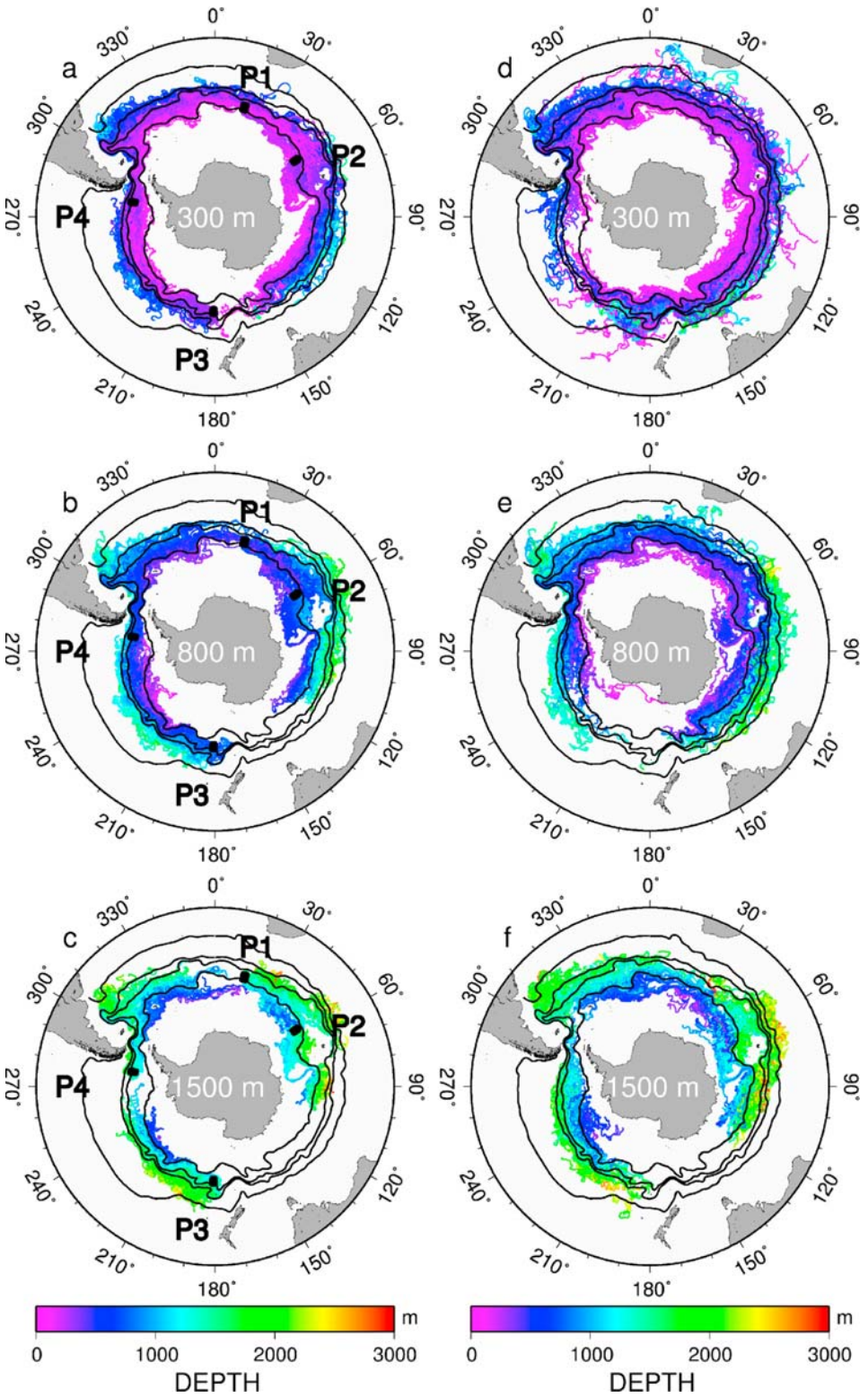

Figure 1. (left) Trajectories after floats have traveled for 3 years (1045 days) in 1998–2000 (Period 1), and deployment locations for the four patches (P1–P4) at deployment depths (a) 300, (b) 800, and (c) 1500 m. (right) Trajectories for days 1046–1761 in 1999–2000 (Period 2), and deployment locations for the four patches (P1–P4) at deployment depths (d) 300, (e) 800, and (f) 1500 m. Color is float depth. Also shown are geostrophic streamlines $\Psi_g = gf^{-1}\eta$ that enclose the approximate location of the ACC. Streamlines were computed using the model's 1998–1999 mean sea surface height η and filtered with a 51-point triangular filter (equivalent to 5°). Streamlines indicate from north to south the approximate mean location of Subtropical Front, Subantarctic Front, Polar Front, and Southern ACC Front.

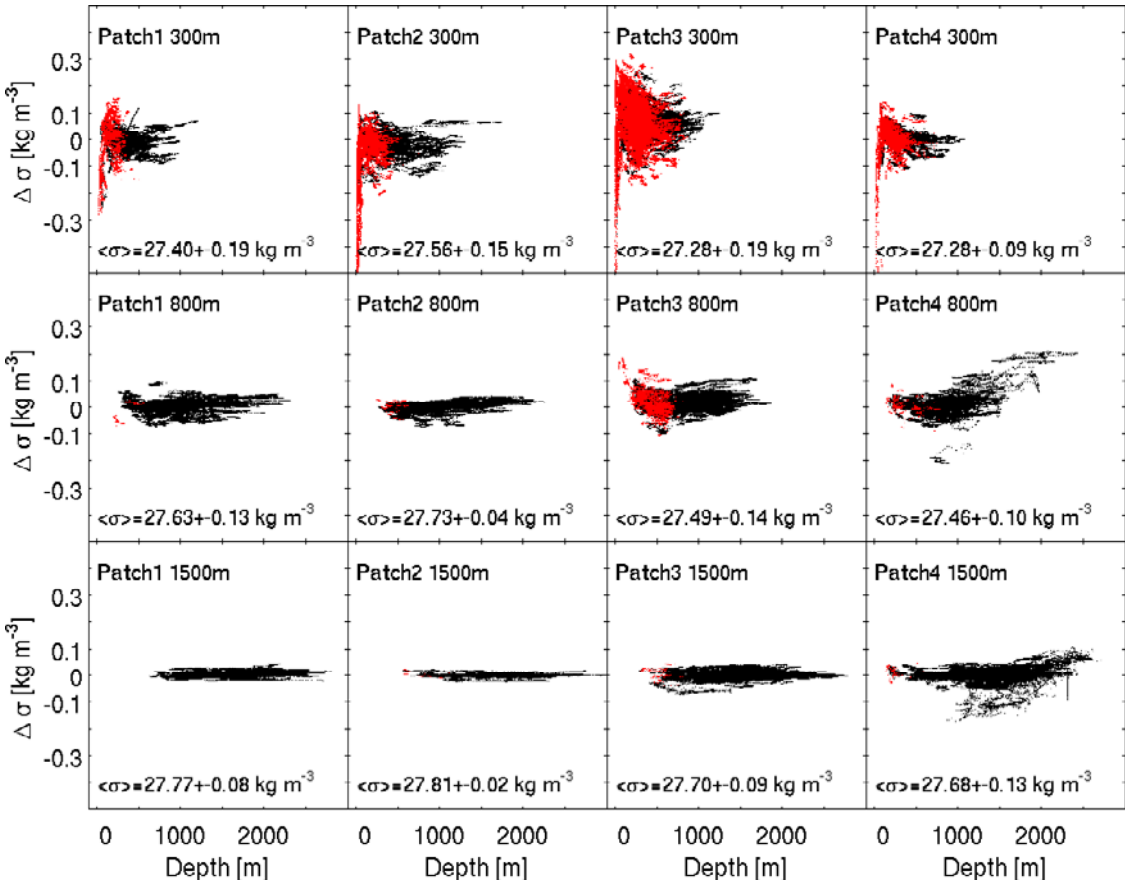

Figure 2. Potential density anomaly $\Delta\sigma$ (kg m^{-3}) for each float point as a function of depth for the first 1045 days (Period 1) using all deployments. Also indicated are the mean potential density and standard deviation for each deployment. Patch numbers 1–4 and deployment depths 300, 800, and 1500 m are shown. Red dots indicate floats have entered the mixed layer.

chosen to allow the floats to move somewhat independently. Closer spacing was judged unlikely to yield additional information, because submesoscale processes are not resolved in the model. For the same reason, high-frequency dispersion statistics might not be expected to be fully representative of the ocean. A first group was deployed on 1 January 1998 and a second group at the same locations 60 days later on 2 March 1998. Here, floats for the two deployments will be combined, since statistically consistent convergence properties, error bars and diffusivities are found from each deployment. After deployment, the floats were advected by the three-dimensional model flow. Trajectory positions were computed using a predictor-corrector scheme with a time step of 6.3 min corresponding to the tracer time step. At midnight each day, temperature, salinity and velocities were interpolated to the current trajectory positions and saved.

[11] The first group of floats traveled for a total of 1761 days (almost 5 years), and the second group traveled for 1701 days. After day 1045 (almost 3 years), the model was restarted at day 1 January 1999. The final locations from the first 1045 days were used as initial conditions for the next 716 days (almost 2 years) for both groups. The reinitialization leads to a discontinuity in the temperature and salinity fields and a less significant one in the velocity fields. Therefore, we treat the trajectories from days 1–1045 and those from day 1046–1761 separately and denote them Period 1 and Period 2 respectively. Figures 1a–1c show the trajectories of all floats for the three deployment depths until day 1045 (Period 1). Figures 1d–1f show the trajectories for days 1045 to 1761 (Period 2). During the first three years most floats stay within the boundaries of the ACC (Figures 1a–1c). During Period 2 a few floats deployed at 300 m upwell and cross the ACC at the surface (Figure 1d).

2.2. How Isopycnal Are the Floats?

[12] If the floats approximately follow isopycnal surfaces they travel to deeper depths when they are north of their deployment location and to shallower depths when they are to the south (Figure 1). Figure 2 shows potential density anomalies as a function of float depth, with respect to the initial potential density for each float, for all patches and deployment depths. Only Period 1 floats are considered, since, as mentioned, the reinitialization led to a discontinuity in the density fields. The labels in Figure 2 indicate the mean potential density (averaged over all floats over the 1045 float days) and the standard deviation. The standard deviation reflects three factors. Some of the variability (O(10^{-2}kg m^{-3})) can be explained by the quarter degree spacing used for the float deployment grid, which means that the floats do not all start at precisely the same density. The different initial conditions in the two groups that were

deployed 60 days apart contribute very little to the standard deviation. The largest part of the standard deviation is due to the fact that potential density is not perfectly conserved along the individual float trajectories. However, the individual floats in the 800 m deployments experience anomalies smaller than 0.2 kg m^{-3} and the 1500 m deployments experience anomalies smaller than 0.1 kg m^{-3}. The trajectories of the 800 and 1500 m deployments in Patches 1 and 2 are more constrained by topography and experience less density change than those in Patches 3 and 4. Patch 2 floats, for example, have to travel through a narrow strait around Kerguelen Plateau, whereas the floats from Patch 3 travel more freely across the abyssal plains west of Drake Passage.

[13] Each float experiences density changes once it encounters the surface mixed layer (indicated in red in Figure 2). Here, the base of the mixed layer is defined as the depth at which the monthly mean potential density differs from surface density by 0.03 kg m^{-3}. Mixed layer encounters occur for 15–30% of the float days for the 300 m deployments, 1–4% for the 800 m deployments, and less than 0.5% for the 1500 m deployments. In this study, we exclude all data from a given float after it encounters the surface or the mixed layer. Away from the mixed layer, density is changed through diapycnal mixing arising from explicit and implicit diapycnal diffusion, and from the resolved diapycnal eddy velocities. A detailed investigation about the origin of the density anomalies requires the use of additional data and must be left to future work.

3. Method

[14] *Davis* [1991] showed how the evolution of the mean tracer concentration in inhomogeneous flows with finite scale eddies depends only on the initial condition of the mean and source fields and the single particle statistics (see Appendix A). For times longer than the typical eddy scales, the eddy flux at time t and location x can then be approximated by a typical flux-gradient relationship with a diffusivity κ^{∞}. This diffusivity is determined by the integral of the Lagrangian autocovariance function

$$\kappa_{ij}(\mathbf{x},\tau) = \int_{-\tau}^{0} d\tilde{\tau} \langle u'_i(t_0|\mathbf{x},t_0)\, u'_j(t_0+\tilde{\tau}|\mathbf{x},t_0)\rangle_L, \qquad (1)$$

$$\kappa_{ij}^{\infty} = \lim_{\tau\longrightarrow\infty} \kappa_{ij}(\mathbf{x},\tau), \qquad (2)$$

where $u'_i(t_0 + \tau|\mathbf{x}, t_0)$ denotes the residual velocity of a particle at time $t_0 + \tau$ passing through x at time t_0 (see Appendix A). $R_L = \langle u'_i(t_0|\mathbf{x}, t_0)\ u'_j(t_0 + \tilde{\tau}|\mathbf{x}, t_0)\rangle_L$ is the Lagrangian autocovariance, and $\langle\ \rangle_L$ is the Lagrangian average over many trajectories (Figure A1). For stationary and homogeneous statistics, the diffusivity is equal to half the time rate of change of the dispersion $\langle r'^2\rangle$

$$\kappa_{ij}(\mathbf{x},\tau) = \frac{1}{2} d_t \langle r'_i(\tau|\mathbf{x},t_0) r'_j(\tau|\mathbf{x},t_0)\rangle_L, \qquad (3)$$

where $r'(\tau|\mathbf{x}, t_0)$ is the displacement at time τ from its starting position, with the mean displacement removed. The definition of the diffusivity in equation (2) is nonlocal, since the time lag τ needs to be long enough for the diffusivity to converge.

[15] Equation (1) requires that the float velocities be separated into mean and eddy components [*Davis*, 1987]. The time-averaged Eulerian mean velocities are highly inhomogeneous in space. Therefore, if we remove a spatially uniform average from each float velocity, we are left with a residual due to the mean shear that will imply dispersion and may dominate the diffusivity estimate [*Bauer et al.*, 1998]. As shown by *Oh et al.* [2000], in a shear flow the along-stream diffusivity is affected by the shear dispersion. *Oh et al.* [2000] and *Zhurbas and Oh* [2003, 2004] assume that the velocity field can be decomposed into the large-scale inhomogeneous mean and a slowly varying and locally isotropic eddy field, implying that eddy mixing could be represented by a single scalar diffusivity. In the presence of shear flow, they suggest using the minor principal component of the diffusivity tensor κ_{ij} as a robust diffusivity that remains unbiased by the shear. This works if the mean shear is homogeneous over the region or bin considered, which is not the case here. Instead, we regard the diffusivity estimated from the local projection across streamlines as a robust diffusivity that ideally is not influenced by the shear. The residual velocity u' from equation (1) is estimated by subtracting the spatially varying Eulerian 1998–1999 time mean velocities from each individual float velocity, which minimizes the shear dispersion in the along-stream direction. This approach works well with numerical model output but would likely be difficult to implement using in situ float observations for which no Eulerian mean is available. We then follow an approach similar to that of *LaCasce* [2000], who projected the individual float velocities across and along f/H contours. We project each residual float velocity locally across and along the spatially varying Eulerian 1998–1999 time mean velocities. By construction this ensures that the cross-stream dispersion by the mean is zero.

4. Diffusivities and Dispersion as a Function of Time Lag

4.1. Long-Time Dispersion and Diffusivities

[16] The purpose of this section is to explore the convergence properties of the Lagrangian diffusivities and discuss their sensitivity to the choice of mean flows, streamline projections and rotational components of the flow. The subtraction of the Eulerian mean velocity from each float velocity allows us to consider the long-time dispersion of each deployment in both the along-stream and cross-stream direction (section 4.1). In oceanic flows with finite eddy scales, equation (1) and (3) entail two regimes of dispersion. Initial dispersion is characterized by a diffusivity that depends on the time lag. After some time T_L, the dispersion is in a random walk regime, which means it is described by a constant diffusivity κ_∞ and a dispersion that is linear with the time lag. The long-time dispersion allows us to assess whether a diffusive limit can be reached and when this occurs. We consider the longest possible time lag and largest number of floats available for each patch and deployment depth. Here we analyze Period 1 only, since trajectories can then be considered to be on the same isopycnal for each patch and deployment depth.

[17] Figure 3 illustrates the influence of coordinate orientation on the long-time dispersion of the Patch 3 300 m deployment (Period 1). As *LaCasce* [2000] found, the dis-

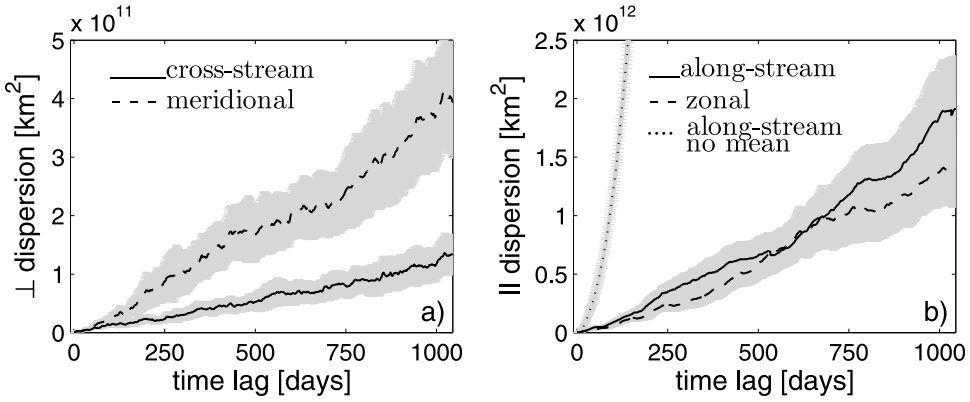

Figure 3. Long-time (1045 days) mean square displacement for Patch 3 for the 300 m deployments, (a) in the cross-stream (solid line) as compared to meridional (dashed line) direction and (b) in the along-stream directions (solid line) as compared to zonal (dashed line) direction. Also shown in Figure 3b is the along-stream dispersion that arises when no mean is subtracted (dotted line). Shaded are 2× standard deviations from bootstrapping by subsampling the floats for each deployment with replacement. Note that in the cross-stream direction the dispersion by the mean is zero by construction.

persion is more anisotropic when it is decomposed into cross-stream and along-stream components rather than meridional and zonal coordinates (Figure 3). The long-time dispersion in the along-stream direction is about an order of magnitude larger than in the cross-stream direction for the Patch 3 300 m deployment. The subtraction of the local Eulerian mean velocities does not entirely eliminate shear dispersion, especially for the 300 m deployments. However, the 800 and 1500 m deployments are close to a random walk even in the along-stream direction (Figures 5e–5h) and it seems likely that a single scalar diffusivity will not be able to describe the eddy mixing even if shear dispersion is reduced. Anisotropy in particle spreading that cannot be attributed to shear dispersion was also recently found in particle dispersion in the North Atlantic [*Kamenkovich et al.*, 2009]. There is also a larger decrease in dispersion with depth in the meridional direction than in the cross-stream direction (not shown). The high along-stream values of the dispersion leak into the meridional direction whenever the mean flow has a substantial meridional component. The magnitude of the dispersion and diffusivities is therefore sensitive to the streamlines used in the projection. When projected across filtered barotropic streamlines (used for binning and along-streamline averages in sections 4 and 5) the cross-stream dispersion by the mean flow is still substantial. This leads to long-time cross-stream eddy diffusivities about 2 times larger than when projected across the local Eulerian mean velocity. This is because of the high filamentation of the local time mean streamlines, and the fact that floats do not locally follow the barotropic streamlines at all depths. The influence of the mean shear is evident in the along-stream dispersion when no mean is subtracted (dotted line in Figure 3b). The dispersion due to the mean is very large and grows with time lag. It is therefore crucial to subtract the spatially inhomogeneous Eulerian mean velocities in order for the along-stream component of the dispersion to be close to linear (solid line in Figure 3b).

[18] Topography also influences long-time dispersion. Whereas Patch 3 floats are constrained little by topography and travel relatively freely across the abyssal plains west of Drake Passage, the Patch 1 300 m cross-stream dispersion is relatively constant for time lags of 500–1200 days, indicative of the floats passing through the narrow gap around Kerguelen Plateau (Figure 4a).

[19] For most deployments, the cross-stream diffusivity converges to a constant within the error bars after about 100 days, consistent with the random walk regime (Figures 5a–5d). The exceptions are the Patch 1 300 m deployments and the Patch 3 1500 m deployments, where the diffusivity tends to zero after a time lag of 600 days. Cross-stream diffusivities are mostly below 1000 $m^2\ s^{-1}$ with some variation from one deployment to another. Patch 2 exhibits the smallest cross-stream diffusivities around 500 $m^2\ s^{-1}$ for all three depths, indicating that most floats are forced to go southward around Kerguelen Plateau without much chance to disperse freely. There is not much depth dependence detectable in the cross-stream diffusivities.

[20] The along-stream diffusivities (Figures 5e–5h) show more depth dependence than the cross-stream diffusivities (Figures 5a–5d). This may be an indication of shear dispersion by the mean flow still playing a role, especially for the 300 m deployments, since mean flow decreases with depth. The along-stream diffusion for the 800 and 1500 m deployments can be described as a random walk from days 250 to 600, except for the Patch 2 and Patch 4 800 m deployments. The along-stream diffusivities for the 300 m deployments tend to increase and decrease with time lag and exhibit less of a random walk regime. The best convergence properties for the along-stream components within the first 600 days are reached again for the Patch 3 deployments for all three deployment depths.

[21] For both cross-stream and along-stream components in the Patch 1 deployments, the dispersion for the first 250–600 days is well simulated by a constant diffusivity determined at a time lag of 100 days (Figure 4). For all patches and time lags longer than about 600 days, cross-stream

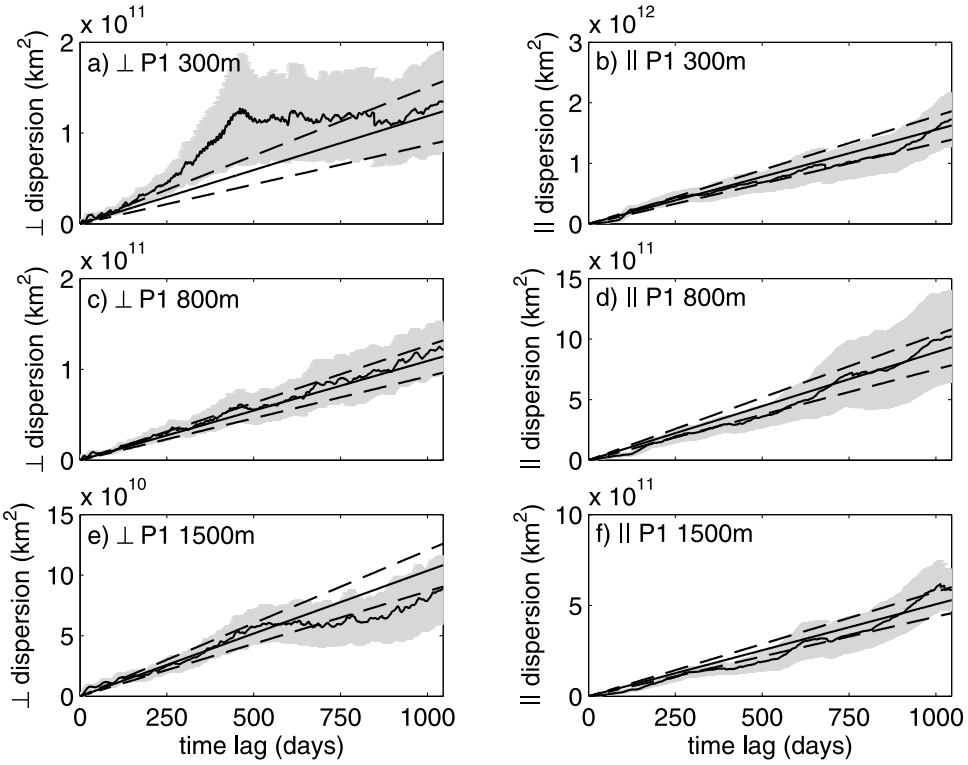

Figure 4. Long-time (1045 days) mean square displacement for Patch 1 for the (a and b) 300, (c and d) 800, and (e and f) 1500 m deployment depths in the (left) cross-stream and (right) along-stream direction. The mean square displacement is compared to the displacement arising when the group of floats disperses with a constant diffusivity taken at time lag 100 days, $\langle r'^2 \rangle_{Taylor} = 2\ \kappa(100d)\ \tau$ (solid lines). The dashed lines and shading are 2σ errors.

dispersion tends to be overestimated by the diffusivity at 100 days time lag (see auxiliary material).[1] Hence, one constant diffusivity does not describe the dispersion for the whole 1045 days, as will be shown in section 5.1, when trajectories are binned geographically.

4.2. Binned Diffusivities as a Function of Time Lag

[22] To resolve the spatial variability of κ_{ij}, we subdivide the domain into bins with the expectation that the bins are larger than the typical eddy scales thus allowing the diffusivities to converge. On the basis of the results from section 4.1, we use a maximum time lag of 90 days, just large enough to be in the random walk regime and small enough to resolve spatial variability.

[23] ACC streamlines are influenced by topography and are therefore not zonally oriented in many areas. We use bins of 10° longitude in the zonal direction, bounded by 7 geostrophic streamlines in the meridional direction. Streamline bins use a natural coordinate system and make it straightforward to average circumpolarly along streamlines. The Eulerian mean velocities used for the projection of the float velocities are spatially nonuniform and cannot be used for constructing streamline bins. Time-averaged barotropic streamlines, $\Psi_g = gf^{-1}\eta$, computed using the model's 1998–1999 mean sea surface height η, also meander substantially and may cross the same longitude multiple times. Therefore, the barotropic streamlines are filtered with a 51-point triangular filter (equivalent to 5 degrees). In Figure 1, the southern edge of the ACC corresponds to the -10×10^4 m^2 s^{-1} streamline, and the northern edge corresponds to the zero streamline. The streamline spacing is $\Delta\Psi_g = 2 \times 10^4$ m^2 s^{-1}. This results in 6 streamline bins, denoted from south to north as bins 1–6. In the following we refer to streamlines 1–2 as south of the Polar Front, streamlines 3–4 as around the Polar Front or core of the ACC, and streamlines 5–6 as north of the Subantarctic Front.

[24] Each daily float observation in each bin is treated as a deployment point from which the float is tracked with positive time lag (arriving at the point) and negative time lag (leaving the point) [*Davis*, 1987, 1991; *Poulain et al.*, 1996; *McClean et al.*, 2002] (also see Appendix A). The Lagrangian average $\langle\ \rangle_L$ in (1) is then the average over all points ending up in the bin.

[25] Floats were released in the core of the ACC, so one can expect the float density to be higher there (e.g., Figure 6a). On the other hand, velocities are highest in the core of the ACC, and streamline bins are therefore smaller (Figure 6b), so the floats do not stay in the bins for long, decreasing the number of float points in these bins. The highest number of float days occurs around Kerguelen Plateau at 70–90°E (Figure 6a), where velocities are small and bin sizes large.

[26] Diffusivites are calculated from equation (1) for positive and negative time lags for all bins. Examples of the cross-stream (Figure 7) and along-stream (Figure 8) diffusivities as a function of time lag are shown for Patch 4 floats

[1] Auxiliary materials are available in the HTML. doi:10.1029/2009JC005821.

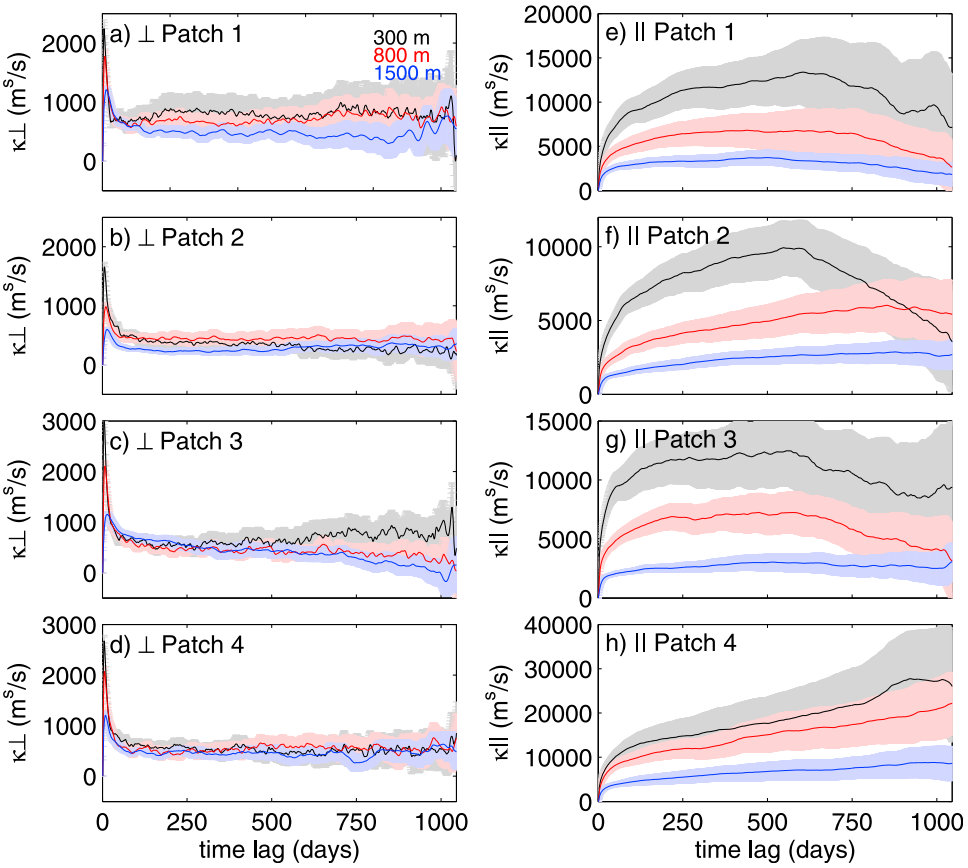

Figure 5. (a–d) Long-time (1045 days) cross-stream diffusivities for all Patches at 300 (black), 800 (red), and 1500 m (blue) deployment depths and (e–h) the same for the along-stream direction. Shaded regions are 2σ errors from bootstrapping by subsampling the floats for each deployment with replacement.

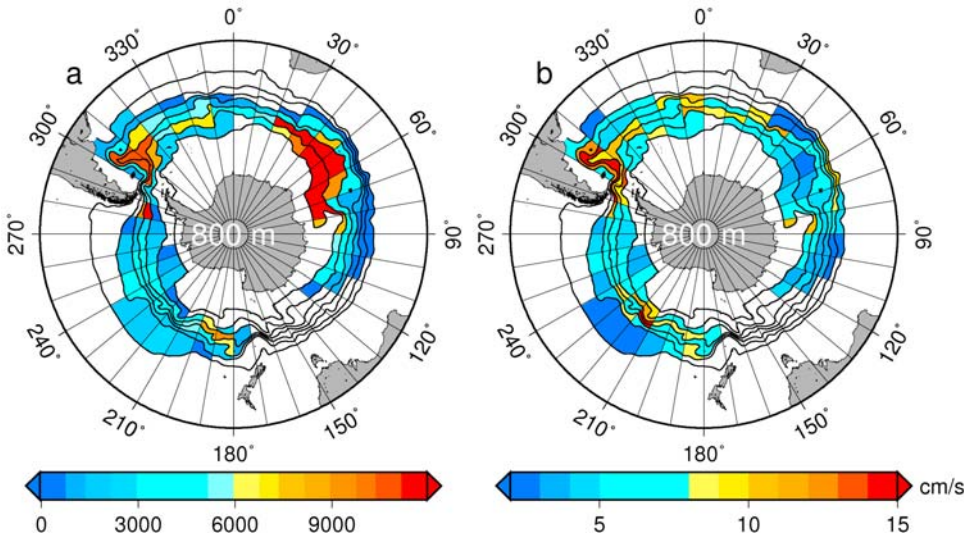

Figure 6. (a) Number of float points per bin for 800 m deployments. (b) Average Eulerian mean velocity (cm s^{-1}) in each bin for the 800 m deployments and trajectories after 1045 days (Period 1). The average was obtained by first interpolating the 2 year Eulerian mean velocity to each float point and then averaging over the bin. Bins are defined at the beginning of section 4.2.

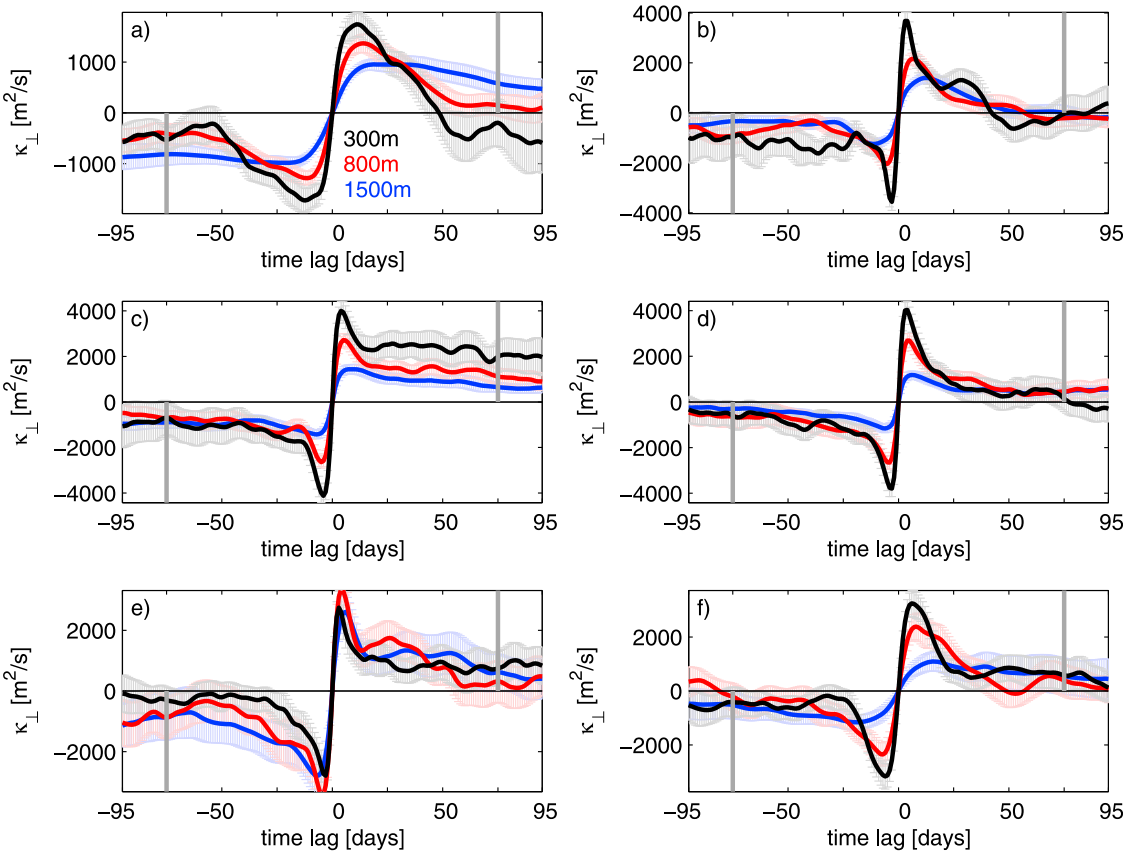

Figure 7. Cross-stream diffusivities as a function of time lag for the Patch 4 at 300 (black), 800 (red), and 1500 m (blue) deployments for streamline bin 3 and longitude bins (a) 290–300°E, (b) 300°–310°E, (c) 310°–320°E, (d) 320°–330°E, (e) 330°–340°E, and (f) 340°–350°E. Also shown are 2σ uncertainties from the bootstrapping. Vertical gray lines indicate the diffusivity at time lag ±75 days.

that are in streamline bin 3 around Drake Passage. Uncertainties are estimated using a bootstrapping process. For each patch and deployment depth, the 160 floats are subsampled 100 times [*Efron and Gong*, 1977]. The subsample has 160 floats, allowing for duplicates. The standard deviations shown in Figures 7 and 8 represent 95% significance levels derived from the subsampling. Generally, the diffusivities in these bins reach a constant value by time lag ±75 days. However, for some bins, the along-stream diffusivites from the 300 m deployments continue increasing after 75 days (Figures 8a–8c). Cross-stream diffusivities show overshoots within the first 10 days and some oscillating behavior particularly for the 300 m deployments (Figure 7) indicating negative lobes in the autocovariance functions (discussed below).

4.3. Defining κ_∞

[27] Lagrangian diffusivity represents diffusion accurately in the ideal scenario of finite scale eddies and homogeneous statistics. In the realistic scenario considered here, both spatial inhomogeneity and nonstationarity introduce potential biases in the estimates of the horizontal and vertical eddy diffusivity distributions.

[28] As discussed in sections 4.1 and 4.2, the along-stream velocity autocovariance integral converges only if we subtract the spatially varying time mean instead of a constant bin mean. Moreover, the eddy field contains rotational components [e.g., *Marshall and Shutts*, 1981], leading to looping and meandering trajectories, that influence the tail of the velocity autocovariances [see, e.g., *Berloff and McWilliams*, 2002a, 2002b; *Veneziani et al.*, 2004, 2005a, 2005b]. As discussed by a number of authors [e.g., *Marshall and Shutts*, 1981; *Jayne and Marotzke*, 2002; *Eden et al.*, 2007; *Griesel et al.*, 2009], the rotational parts of the eddy fluxes do not contribute to the local heat budget. Therefore, they should have no net particle dispersion and zero Lagrangian diffusivity κ^∞.

[29] When floats travel through meanders or circle around stationary eddies, this leads to oscillatory patterns in the autocovariance and diffusivity, as illustrated in Figure 9. This effect was also discussed by *Berloff and McWilliams* [2002a] and by *Veneziani et al.* [2004, 2005a, 2005b]. Figures 9a–9c considers an idealized scenario of particles circling twice around eddies and meandering in a half circle. These rotational motions do not contribute to the diffusivity at time lags longer than the meander or circling time scale. Superimposed on this rotational field is a random velocity field with a decorrelation scale of 10 days. For the half circle meanders, diffusivity as a function of time lag grows first, reaches a maximum and then declines again before it returns (by time lag 10 days) to the correct asymptotic value as determined only by the random component of the velocity field (Figure 9c). The net cross-stream dispersion of the float due to the meanders and circles is zero. In a more

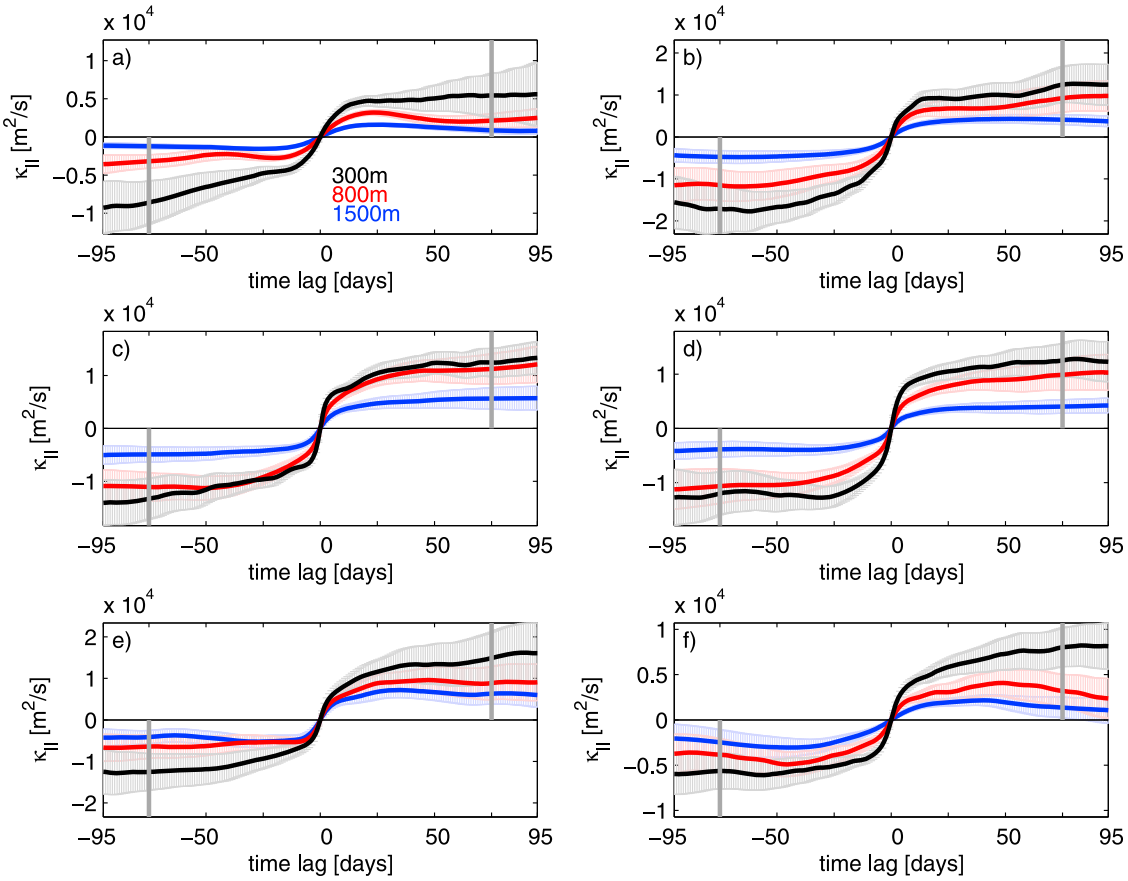

Figure 8. Along-stream diffusivities as a function of time lag for the Patch 4 at 300 (black), 800 (red), and 1500 m (blue) deployments for streamline bin 3 and longitude bins (a) 290–300°E, (b) 300°–310°E, (c) 310°–320°E, (d) 320°–330°E, (e) 330°–340°E, and (f) 340°–350°E. Also shown are 2σ uncertainties from the bootstrapping. Vertical gray lines indicate the diffusivity at time lag ±75 days.

realistic scenario of a complex eddy field that consists of eddies of different sizes that grow and decay (Figure 9d), velocity autocovariance functions will show more complex oscillatory behavior (Figure 9e). One question is whether the oscillatory behavior is transient and the diffusive limit can be reached, as in the idealized scenario of Figures 9a–9c and in the long-time dispersion. If more independent trajectories are considered in the Lagrangian average, then the oscillations in the tail of the autocovariance are more likely to cancel each other. The full group of floats in section 4.1 for example, shows little oscillatory behavior after about 50 days (Figure 10). However, there still is a maximum diffusivity in the 0–10 day time lag interval that is about 2–4 times larger than κ^∞ (Figure 10). This maximum may reflect the scale of the meandering current and does not disappear or average out when more and more floats are considered that are subject to the same meander scale.

[30] A standard practice to determine κ^∞ in equation (2) is to integrate the autocovariance functions to the first zero crossing [e.g., *Freeland et al.*, 1975; *Krauss and Böning*, 1987; *Poulain and Niiler*, 1989; *Lumpkin et al.*, 2001]. This works if the trajectories in the eddy field are not dominated by looping or meandering patterns. Alternatively, idealized covariance functions that asymptote to zero are fitted to the observed covariance functions [e.g., *Garaffo et al.*, 2001; *Sallée et al.*, 2008]. *Lumpkin et al.* [2001] compared several different methods to determine κ^∞. They found that the integration of the autocovariance until the first zero crossing leads to higher eddy scale estimates in the region of the Gulf Stream than when an idealized autocovariance consisting of exponentially decaying and wave components is fitted to the data and integrated to infinity. The integration of R_L until the first zero crossing is equivalent to taking the maximum of the diffusivity as a function of time lag in the cross-stream direction. As shown in Figure 9f, the maximum of the diffusivity is not the right measure for the dispersion. The negative and positive lobes after the maximum cannot be neglected in the integration of the covariance.

[31] The most accurate determinations of the asymptotic diffusivity are made by estimating $\kappa(\tau)$ at the smallest lag for which $\kappa(\tau) = \kappa_\infty$ [e.g., *Davis*, 1991; *Swenson and Niiler*, 1996]. We therefore estimate the diffusivity κ^∞ for all bins as an average of the diffusivity at time lags +75 days and −75 days. The 75 day integral is chosen as it represents the smallest timescale when most of the diffusivities for the bins are expected to be in the random walk regime and to have reached a plateau (e.g., Figure 10, and compare also Figure 5). This timescale is substantially larger than the ≈5–10 day timescales typical of the first zero crossing of our Lagrangian cross-stream velocity autocovariance.

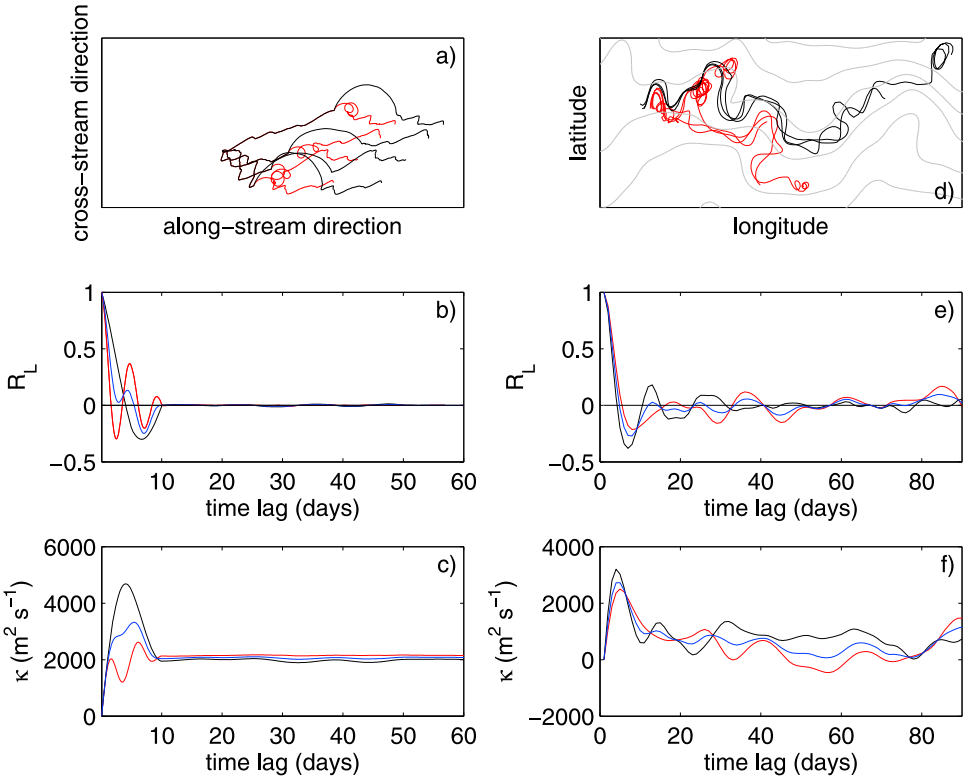

Figure 9. (left) Idealized scenario; random velocity field plus constant mean flow in along-stream direction, superimposed on particles passing through a half circle meander (black) and circling twice around a stationary eddy (red) (see Appendix B for details). (a) Idealized trajectories. (b) Velocity autocovariance in cross-stream direction for particles passing through the half circle meander (black), circling around the eddy twice (red) and the average of these two scenarios (blue). (c) Corresponding cross-stream diffusivities as a function of time lag. (right) Examples from the POP float deployments. (d) Examples of circling and meandering numerical trajectories from the Patch 2 at 300 m deployment. (e) Corresponding velocity autocovariance. (f) Diffusivities as a function of time lag.

[32] Unlike the cross-stream diffusivities (Figure 7), the along-stream diffusivities (Figure 8) do not exhibit oscillatory behavior, and the maximum in the 0–90 day time lag interval is equal to $\kappa_{\parallel}^{\infty}$. This may be due to the fact that while a full circle trajectory does not lead to any net dispersion in the along-stream direction, meandering trajectories do lead to net along-stream dispersion and no oscillatory behavior. On average, meanders, rather than the circling trajectories, may dominate the time lag dependence of the Lagrangian diffusivities. Cross-stream diffusivities are much smaller than along-stream diffusivities and the strong rotational effects are more likely to overwhelm the cross-stream diffusivities.

5. Lagrangian Diffusivities and Their Relationship to Eddy Kinetic Energy, Eddy Scales, and Mean Flow

[33] While the results of section 4 show that cross-stream diffusivities converge to stable values over 100–1000 day average intervals, averaging along extended trajectories does not allow us to consider spatial patterns or to examine how they may vary as a function of depth. In order to assess geographic variation in diffusivity, in section 5.1 we bin data geographically, and in order to assess vertical struc-

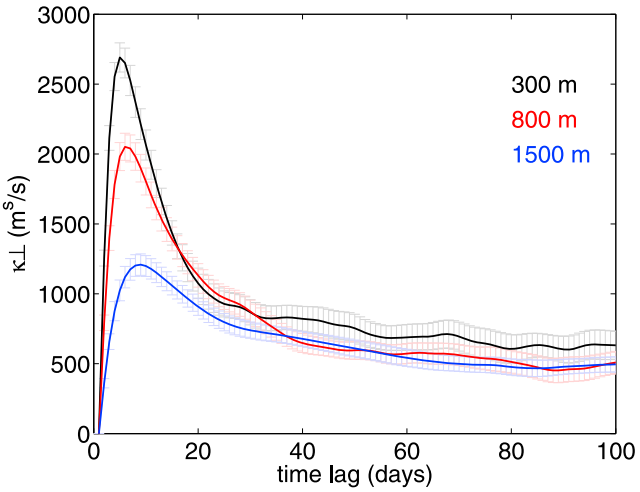

Figure 10. Enlargement for the first 100 days of the cross-stream diffusivities as a function of time lag for Patch 4 (Figure 5d).

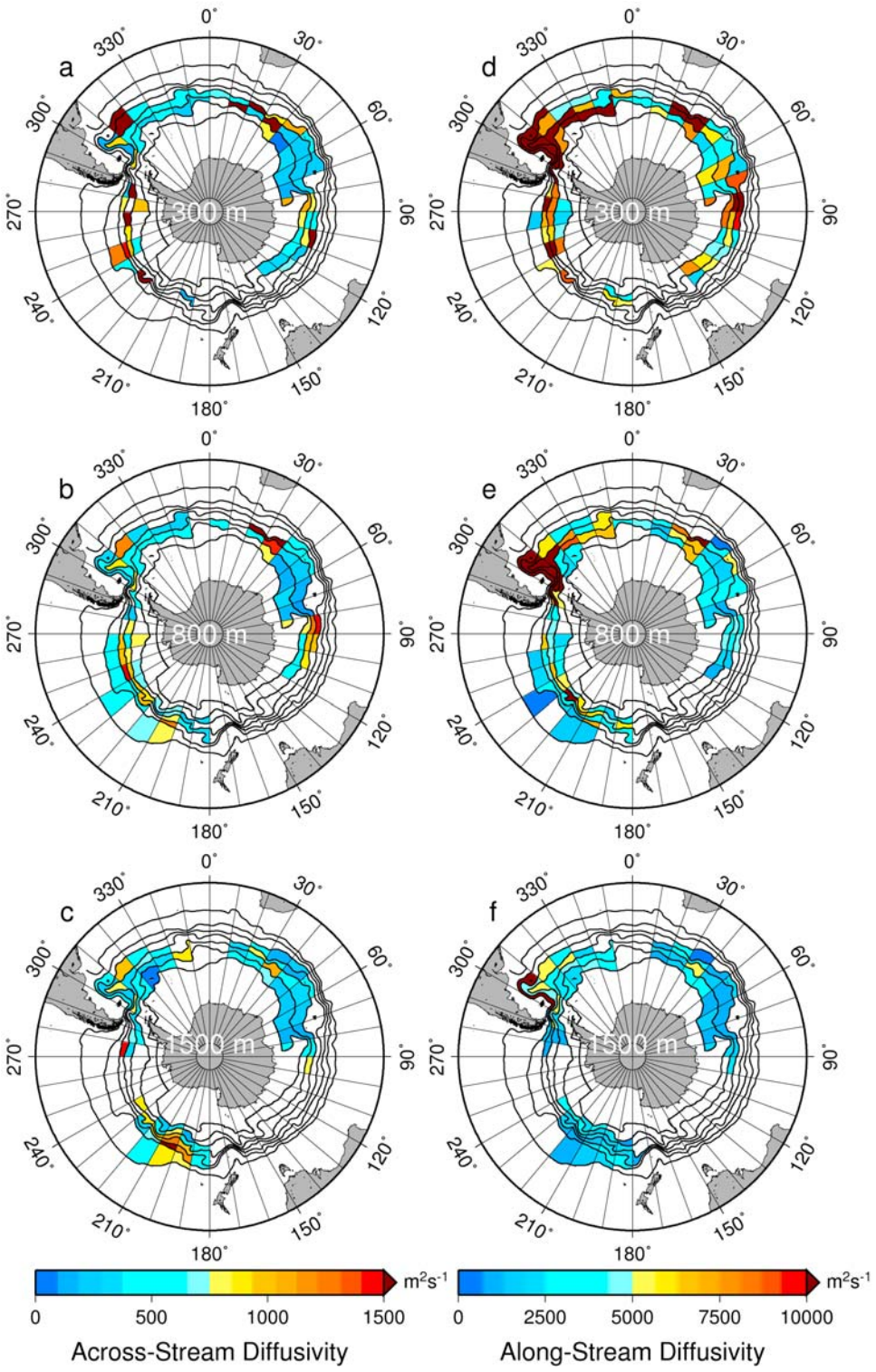

Figure 11. (left) Cross-stream and (right) along-stream diffusivities ($m^2\ s^{-1}$) for the deployment depths of (a and d) 300 m ($\overline{\sigma_0} = 27.36 \pm 0.61$ kg m^{-3}), (b and e) 800 m ($\overline{\sigma_0} = 27.58 \pm 0.27$ kg m^{-3}), and (c and f) 1500 m ($\overline{\sigma_0} = 27.74 \pm 0.20$ kg m^{-3}) for 1 to 1045 day trajectories (Period 1). In a few cases where bins of different deployments overlapped, diffusivities were averaged. Standard errors for the cross-stream diffusivities are on average 30% of the diffusivity for the 300 m deployments and about 10% of the diffusivity for the 800 and 1500 m deployments. Standard errors for the along-stream diffusivities are on average 20% of the diffusivity for the 300 m deployments and about 10% of the diffusivity for the 800 and 1500 m deployments.

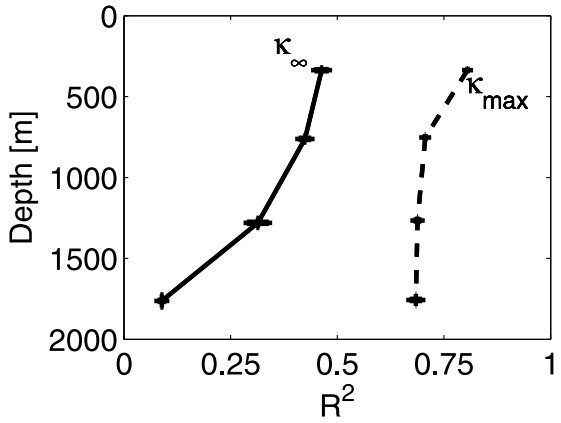

Figure 12. Correlations between cross-stream diffusivities (κ) and eddy velocities ($\sqrt{\langle u'^2 \rangle}$) as a function of mean depth, under consideration of all trajectories (Period 1 and 2). R^2 is the variance explained by the linear regression model devided by the total variance of the data. Solid line is κ_∞. Dotted line is κ_{max}. Here κ_{max} is obtained by taking the maximum of the diffusivity in the 0–75 day time lag interval, which in the cross-stream direction is equivalent to integrating the Lagrangian autocovariance R_L to the first zero crossing. Error bars are standard errors from bootstrapping by subsampling the floats in each depth interval with replacement.

ture in section 5.2 we sort the float trajectories into 4 depth intervals.

5.1. Horizontal Distributions

[34] By averaging the data in geographic bins, we are able to evaluate horizontal distributions of the diffusivities κ^∞ at each deployment depth. Since there is a discontinuity in the density field at day 1045, we consider only the trajectories for Period 1. This means that horizontal distributions of diffusivities are on isopycnal surfaces that are relatively constant for each of the deployments (compare Figure 2). Only bins with a minimum of 1500 daily float positions are considered, ensuring 'convergence' properties as in Figures 7 and 8. When fewer than 1500 float positions are available we find that convergence is not reliably achieved, especially for the 300 m deployments. Since most floats do not cross the Subantarctic Front, streamline bin 6 only has significant data for longitudes between 180°E and 250°E (Figure 6). After 1045 days, the floats have not traveled far enough from any of the initial deployment patches to sample the region south of Australia and New Zealand (Figures 1b and 1c). Also, in some bins float density is reduced due to mixed layer encounters in the 300 m deployments, for example 180°E–220°E (Figures 11a and 11b).

[35] Horizontal patterns of cross-stream and along-stream diffusivities for the three deployment depths are inhomogeneous: the latitude dependence varies with geographic location, and diffusivities can have local maxima and minima in the core of the ACC jet (Figure 11). Note that similar horizontal distributions for three depth intervals, instead of deployment depths, are found in Figure S4 in the auxiliary material. The relatively high spatial variability in Figure 11 was not evident in the long-time diffusivity estimates from section 4.1. In the east Pacific sector of the Southern Ocean where the flow crosses the abyssal plains, cross-stream diffusivities are high in the core of the ACC jet (see also Figure 6). West of 0°E cross-stream diffusivities are lower in the core of the ACC (see also Figure S4 in the auxiliary material). The highest cross-stream diffusivities, exceeding 2500 $m^2\ s^{-1}$, are found south of the Agulhas Retroflection and near the Brazil-Malvinas confluence zone. High values are also found where the flow veers around islands or topographic features, such as the Kerguelen Plateau (70°–90°E) and Chatham Rise south-east of New Zealand (180°–190°E).

[36] Along-stream diffusivities are about 3–10 times larger than cross-stream diffusivities (Figure 11). Along-stream and cross-stream diffusivities are generally not correlated. However, areas of high along-stream diffusivities generally would appear to coincide with areas of enhanced cross-stream diffusivities if the float velocities were represented in zonal and meridional coordinates or if they were projected into along-stream and cross-stream coordinates using filtered barotropic streamlines rather than local time-averaged velocities. In these cases there is leakage of the high along-stream (or zonal) values into the cross-stream (or meridional) terms. The largest values of along-stream diffusivity, exceeding 10,000 $m^2\ s^{-1}$, occur in the Brazil-Malvinas confluence zone and north of the Kerguelen Plateau.

[37] What factors determine the horizontal distributions of the diffusivities? Both eddy kinetic energy and eddy length scales have been hypothesized to govern diffusivity variations. These two quantities are not independent, since eddy length scales can depend on eddy kinetic energy. The Lagrangian diffusivity can be thought of as the product of the Lagrangian average of the eddy velocity $\sqrt{\langle u'^2 \rangle}$, and the Lagrangian eddy length scale L_L, or alternatively, as the product of the Lagrangian average of the squared velocity $\langle u'^2 \rangle$ and the characteristic Lagrangian eddy time scale $T_L = L_L/\sqrt{\langle u'^2 \rangle}$. The Lagrangian eddy scales are obtained from the integral of the velocity autocovariance. In other words, the diffusivity is determined by the Lagrangian averaged velocity autocovariance at zero lag and by the structure of the tail of the Lagrangian autocovariance for time lags > 0. If either the Lagrangian time scales or the Lagrangian length scales could be considered constant, then the spatial distributions of the diffusivities would be determined by the eddy velocities or eddy kinetic energies. No consistent relationship between Lagrangian diffusivities and eddy kinetic energy or eddy velocity has been found in numerous studies using floats from many areas in the ocean (see, e.g., *Lumpkin et al.* [2001] for an overview), suggesting no universal constant L_L or constant T_L rules.

[38] Figure 12 shows that the correlation of the Lagrangian diffusivities with the eddy velocities can be quite different depending on what time lag is used for the integration of the velocity autocovariance. Only about 50% of the horizontal distributions of κ^∞ can be explained by variation of the eddy velocity in the surface depth interval, and only about 10% for the 1500–2500 m depth interval. Clearly, the Lagrangian eddy length scale cannot be considered constant especially for the deeper depth levels. On the other hand, when we use κ_{max} as the measure for the

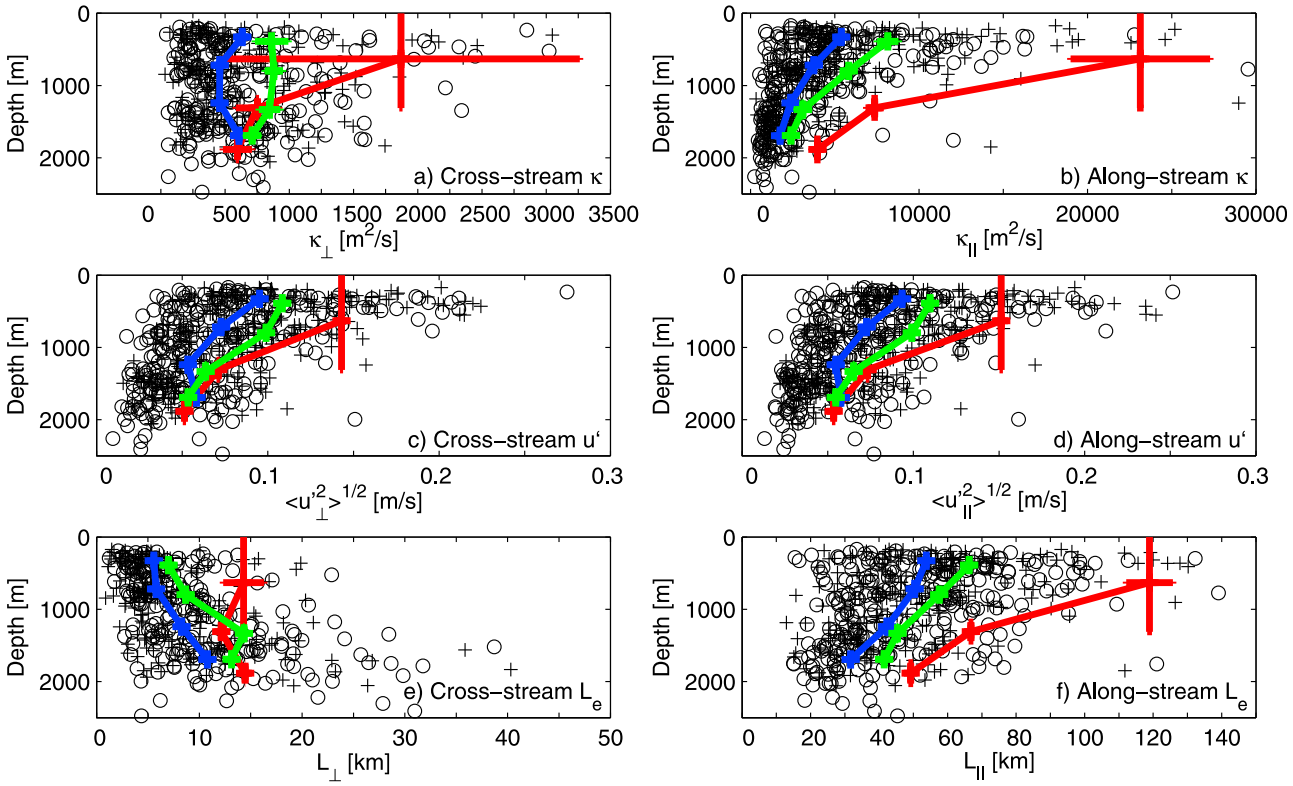

Figure 13. (a) Cross-stream diffusivities ($m^2\ s^{-1}$), (b) along-stream diffusivities ($m^2\ s^{-1}$), (c) across-stream eddy velocity $\langle u_\perp^2 \rangle$ ($m\ s^{-1}$), (d) along-stream eddy velocity $\langle u_\perp^2 \rangle$ ($m\ s^{-1}$), (e) cross-stream eddy length scale (km), and (f) along-stream eddy length scale (km) as a function of mean bin depth. Pluses indicate results from the 1–1045 day trajectories (Figure 1 (left)) and circles indicate bins for the 1046–1761 days trajectories (Figure 1 (right)). The three vertical lines are along-streamline averages as a function of mean depth intervals 5–500, 500–1000, 1000–1500, and 1500–2500 m over the streamline intervals 1–2 (blue, south of Polar Front), 3–4 (green, around Polar Front), and 5–6 (red, north of Subantarctic Front) from south to north.

Lagrangian diffusivity, we find misleading high correlations with eddy velocity, which could lead to false conclusions that eddy length scales may be considered constant and that eddy velocities or eddy kinetic energies may be used to determine the spatial distributions of the diffusivities. Note that similar correlation patterns and differences for κ^∞ and κ_{max} are found when the cross-stream diffusivity is correlated with the eddy kinetic energy, instead of the eddy velocity. Also, the along-stream diffusivity is highly correlated with the eddy velocities or eddy kinetic energies (not shown).

[39] Neither the eddy length nor the eddy time scale can be considered horizontally homogeneous in the cross-stream direction, suggesting that parameterizations of eddy diffusivity that depend solely on eddy kinetic energy are likely to be incomplete.

5.2. Depth Dependence

[40] We now assess the vertical structure of the diffusivities as a function of mean bin depth, without regard for the isopycnal on which the floats were initially launched. All float trajectories from the left and right panels of Figure 1 (Periods 1 and 2) are considered in this section. The spread of the individual cross-stream (Period 1 pluses and Period 2 circles in Figure 13a) and along-stream (Figure 13b) diffusivity estimates as a function of depth shows that the flow regimes vary with longitude and latitude (Figure 11). In general, the along-stream averaged diffusivities increase northward, although this increase becomes less significant with depth. As shown in the previous section, this latitude dependence is not constant for all longitudes. At some longitudes, local diffusivity maxima occur in the core of the ACC jet with smaller diffusivities to the north, for example west of Drake Passage (240°E–280°E). For the northernmost streamlines (red line in Figure 13), cross-stream diffusivities are $1800 \pm 1200\ m^2\ s^{-1}$ for the 500–1500 m depth interval, but in this depth range only 4 bins have significant data (Figure 11). Since the floats travel deeper toward the north, the 0–500 m depth interval was not sampled by the two northernmost streamline bins. Around the Polar Front (green lines in Figure 13), cross-stream diffusivities of between 500 and 1000 $m^2\ s^{-1}$ are fairly uniform with depth. The depth dependence is more pronounced for along-stream diffusivities and is what one might expect if diffusivity were correlated with eddy kinetic energy and eddy transports, decreasing with depth. Lagrangian diffusivities (Figures 13a and 13b) show no evidence of a maximum at depth, in contrast with predictions of critical layer theory [*Green*, 1970; *Smith and Marshall*, 2009].

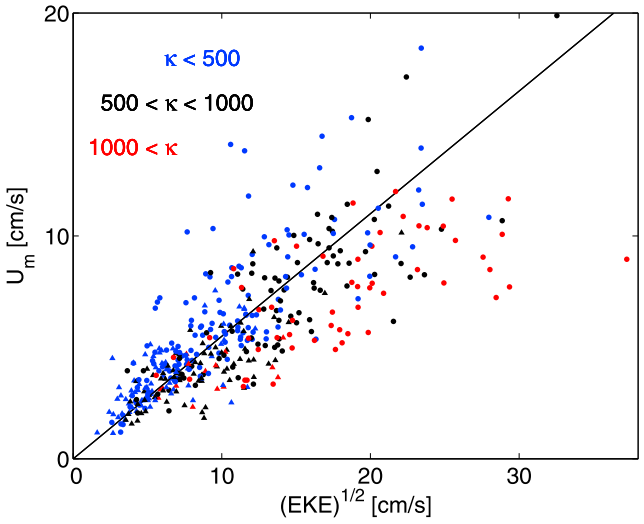

Figure 14. Eulerian mean velocity as a function of eddy kinetic energy averaged over each bin. Across-streamline diffusivity values are in color for three intervals (<500 m^2 s^{-1} (blue), between 500 and 1000 m^2 s^{-1} (black), and >1000 m^2 s^{-1} (red)). In the upper ocean within the ACC, $u_m - c \approx u_m$. For the 1500 m deployments (triangles), using $u_m - c$ would be more appropriate.

[41] Whereas in the previous section we considered the importance of the horizontal distributions of the eddy velocity and eddy scales for determining the horizontal distributions of diffusivities, we now investigate the relative importance of the length scale and eddy velocity in determining the depth dependence of the diffusivities. A decrease of diffusivities with depth was expected when diffusivities were correlated with eddy kinetic energy. Figures 13c and 13e shows the cross-stream eddy kinetic energy component and eddy length scale and Figures 13d and 13f the along-stream eddy velocity and length scale as a function of mean bin depth. The cross-stream and along-stream eddy kinetic energy components (Figures 13c and 13d) are comparable in their magnitudes and distributions, indicating isotropic eddies. For the cross-stream direction, the interplay between eddy length scales increasing with depth (Figure 13e) and eddy velocities decreasing with depth (Figure 13f) leads to eddy diffusivities (Figure 13a) that are relatively constant with depth. The along-stream eddy length scales decrease with depth, especially north of the Subantarctic Front (red line). Overall, the analysis demonstrates that a parameterization of diffusivity that is only related to eddy kinetic energy is incomplete and leads to the wrong depth dependence. For example, the cross-stream eddy velocity in the 1500–2500 m depth interval is only about 30% of its near surface value. In contrast the cross-stream diffusivity is about the same as its near surface value in the 1500–2500 m depth interval around the Polar Frontal Zone.

[42] If the eddy kinetic energy alone does not determine the cross-stream mixing, then perhaps it is the strength of the mean flow that limits mixing and leads to smaller eddy scales?

[43] *Shuckburgh et al.* [2009a, 2009b] reported on average a significant correlation between effective eddy diffusivities and $EKE/(U_m - c)^2$ where U_m is the strength of the mean flow and c is the eddy velocity, illustrating that strong mean flow may limit mixing, at least as long as it is not comparable to the eddy velocity. Similarly to Figure 11 of *Shuckburgh et al.* [2009b], Figure 14 shows the dependence of the Lagrangian cross-stream diffusivity on both the strength of the bin-averaged mean flow and EKE. There is evidence that a stronger mean flow acts as a mixing barrier within the ACC, since high diffusivities tend to be located below the black line in U_m/EKE space, and small eddy diffusivities above the black line towards higher values of mean flow. There are some bins for example with small EKE (around 10 cm s^{-1}) but large Lagrangian diffusivities. However, cross stream dispersion is not consistently reduced in areas with strong Eulerian mean velocities in the ACC. As *Shuckburgh et al.* [2009a] found, we find that the correlation of the cross-stream Lagrangian diffusivities with EKE/U_m^2 is significant ($R^2 = 0.47$) when all bins are taken into account, and slightly lower when the cross-stream diffusivity is just correlated with EKE (cf. Figure 12). On the other hand, the correlation of κ_{max} with EKE/U_m^2 is only 0.32, whereas the correlation with EKE alone is high at 0.76 when all bins are taken into account (cf. Figure 12). Hence, κ_{max} does not detect mixing barriers where the mean flow is strong.

[44] We note that the floats stay mainly within the boundaries of the ACC, and, as mentioned, north of the Subantarctic Front there are no bins in the 5–500 m depth interval and only 4 bins in the 500–1500 m depth interval with statistically significant diffusivities. Therefore, we do not adequately resolve the area north of the ACC, where the mean flow is much weaker and likely Lagrangian diffusivities will be larger in the along-streamline average.

6. Conclusions

[45] We have used numerical floats to estimate horizontal and vertical distributions of Lagrangian diffusivities in the Southern Ocean. Lagrangian cross-stream diffusivities converged to a constant value, provided that the time lag was long enough and that oscillations were minimized by considering enough float points in the Lagrangian average. Along-stream diffusivities also tended to converge, at least for the 800 and 1500 m deployments, provided that a spatially varying time mean was subtracted from the float velocities to minimize shear dispersion. Our results have shown that diffusivities are anisotropic and that a single scalar diffusivity is not appropriate to describe eddy mixing in the ACC. The influence of topography was clearly evident in the long-time dispersion, where a single constant diffusivity did not simulate the dispersion for the whole Period 1, except in the Patch 3 300 and 800 m deployments that were the least constrained by topography.

[46] The diffusivity distributions were analyzed in the context of theories predicting specific depth and latitude dependence. Lagrangian diffusivities are horizontally inhomogeneous and can be high in regions where eddy kinetic energy is high, such as in the Polar Front and to the north of the Subantarctic Front. But the horizontal distributions of diffusivities are not highly correlated with the eddy kinetic energy or eddy velocity, indicating that the Lagrangian eddy length and time scales cannot be considered constant. We have pointed out the substantial differences in cross-stream

Lagrangian diffusivities between κ at the first zero crossing and κ^∞. Not only do the magnitudes of the diffusivities differ between these two estimates but also their spatial distributions. There is a decrease with depth when the maximum κ is taken, because the diffusivities, as a function of time lag, tend to show more oscillatory behavior close to the surface than at depth. In addition, high correlations with eddy kinetic energy in previous studies [*Krauss and Böning*, 1987; *Lumpkin et al.*, 2001; *Zhurbas and Oh*, 2004] might occur because these studies used the maximum of the diffusivities rather than κ^∞. With the more appropriate measure κ^∞, we do not find such high correlations with eddy kinetic energy. Parameterizations that only use eddy kinetic energy to parameterize the diffusivities are therefore incomplete. The Lagrangian near surface cross-stream diffusivities in the core of the ACC jet are more comparable to the *Marshall et al.* [2006] and *Abernathy et al.* [2009] effective diffusivity estimates of close to 500 $m^2\ s^{-1}$. Our diffusivity in the core of the ACC is sensitive to the way the float velocities are projected. We required that the cross-stream dispersion by the mean be zero.

[47] Our cross-stream diffusivities are substantially smaller than those found by *Sallée et al.* [2008] within the ACC. This might be due to the fact that *Sallée et al.* [2008] considered mixing at the surface which includes stronger diapycnal mixing that occurs within the mixed layers and has been excluded in our analysis. Further, they used a different method to separate along-stream and cross-stream mixing. They determined the orientation of the cross-stream direction by using the minor axis of the velocity covariance tensor in each bin. We have taken into account small-scale spatial variation of the Eulerian velocity by projecting across and along the local mean velocity at each point, which greatly reduces the cross-stream diffusivity.

[48] When the time lag is long enough, our Lagrangian diffusivities are correlated with the eddy kinetic energy to mean flow ratio, albeit with a somewhat lower correlation coefficient than for the effective diffusivities of *Shuckburgh et al.* [2009a, 2009b]. The correlation with EKE alone is weaker. Our mean flow represents averages over 10° longitude bins, and there are gaps in the horizontal distribution of the diffusivities due to insufficient Lagrangian data. Therefore, a clearer distinction between stronger and weaker mean flows, which lead to smaller and larger cross-stream dispersion respectively, may not be detected with the single particle dispersion considered here.

[49] Cross-stream eddy diffusivities decrease with depth north of the Subantarctic Front, although the high values close to the surface are only found in a few bins. Along-stream averages of cross-stream eddy diffusivities around the Polar Front are relatively uniform with depth. We did not find support for enhanced mixing due to critical layers below the core of the ACC jet. However, cross-stream eddy length scales did increase with depth, masked by the strong depth decrease of eddy velocities. This might just indicate that eddies are larger at depth but might not mean there is more mixing. *Naveira Garabato et al.* [2009] have recently argued that the eddy mixing length, as defined by, for example, *Armi and Stommel* [1983], determines the spatial distributions of the eddy diffusivities. The question remains how classical eddy mixing lengths and Lagrangian eddy length scales are related.

[50] The depth dependence of our diffusivities is different from the depth dependence of the effective diffusivities obtained from *Abernathy et al.* [2009], who found enhanced values up to 4000 $m^2\ s^{-1}$ below the core of the ACC jet, at depths of 1500 m on average, and small values of about 500 $m^2\ s^{-1}$ in the core of the jet. While Lagrangian and effective diffusivities have similar magnitudes and distributions in the upper ocean, it is unclear why they differ at depth. The effective diffusivity may capture small-scale features due to topographic interactions that the Lagrangian diffusivity can not resolve due to its nonlocalness. If the eddy mixing at depth is highly localized, we simply may not sample the depth interval 1500–2500 m well enough due to the limited amount and extent of the numerical trajectories. Some of the high effective diffusivities from *Abernathy et al.* [2009] occur at depths much deeper than 2500 m, a region that we do not sample at all. Furthermore, in the effective diffusivity method, the passive tracer follows the instantaneous streamlines, and instantaneous cross-stream mixing is evaluated where the rotational part of the eddies plays no role. The tail of the velocity autocovariance for time lags > 0, and therefore the calculation of the Lagrangian eddy scales, is biased by the presence of rotational components and by the problem of identifying appropriate eddy length scales. *Griesel et al.* [2009] have recently evaluated the curl and divergence of the horizontal eddy heat flux in 1/10° POP and found that the rotational components, as measured by the curl, dominate even for averages over scales much larger than the size of the eddies. Extended numerical float deployments are needed in the future to sample all latitudes and depths in the Southern Ocean, and to evaluate further whether the bias of the rotational part can indeed be eliminated in the Lagrangian diffusivity.

Appendix A

[51] The elaborated flux versus gradient law of *Davis* [1987, 1991] and *Poulain et al.* [1996]

$$\langle u_i'(\mathbf{x},t)\Theta'(\mathbf{x},t)\rangle = -\int_0^t d\tau \partial_\tau \kappa_{ij}(\mathbf{x},\tau)\partial_{x_j}\overline{\Theta}(\mathbf{x},t-\tau) \tag{A1}$$

$$\kappa_{ij}(\mathbf{x},\tau) = \int_{-\tau}^0 d\tilde{\tau}\langle u_i'(t_0|\mathbf{x},t_0)\, u_j'(t_0+\tilde{\tau}|\mathbf{x},t_0)\rangle_L \tag{A2}$$

$$As\ \ \tau \longrightarrow \infty : \tag{A3}$$

$$\langle u_i'(\mathbf{x},t)\Theta'(\mathbf{x},t)\rangle = -\kappa_{ij}^\infty(\mathbf{x})\partial_{x_j}\overline{\Theta}(\mathbf{x},t) \tag{A4}$$

specifies the flux of a (passive) tracer Θ from the recent history of its mean concentration. The driving force for the eddy flux at time t is the sum of previous Θ gradients at times $t - \tau$, weighted by the time derivative of κ at time range τ. Here κ is defined as the integral of the time lagged Lagrangian velocity autocovariance. This is an elaboration of the familiar advection-diffusion equation, where the elaboration reflects the finite scales of the eddies. If τ goes to infinity, or, rather, is greater than some time T reflecting the finite scales of the dispersing eddies, $\kappa(x, t)$ approaches a

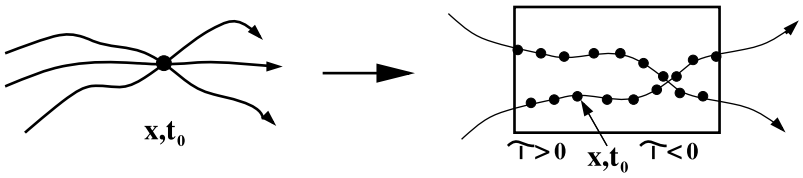

Figure A1. (left) Ideal scenario of an ensemble of particles passing through x at time t_0, which becomes in practice (right) the scenario of floats passing though a space domain or bin. Each daily float observation in the domain is considered as a deployment point from which the float is tracked with positive time lag (arriving at the point) and negative time lag (leaving the point).

constant value κ^{∞} and the eddy flux is approximated by the typical advection-diffusion equation. The Lagrangian average is an average over all particles passing through x, t_o. In theory, we are looking at an ensemble of particles passing through x at time t_0 (Figure A1 (left)). In practice with only one realization of the simulated floats, we are looking at floats passing through a space domain or bin (Figure A1 (right)). Each daily float observation in the domain is considered as a deployment point from which the float is tracked with positive time lag (arriving at the point) and negative time lag (leaving that point). Lagrangian average is then an average over all points passing through the bin.

Appendix B

[52] For illustration purposes we have carried out tests to show the impact of circular eddies on the Lagrangian diffusivity estimates. More detailed analyses with looping trajectories have been carried out by, e.g., *Veneziani et al.* [2004, 2005a, 2005b]. We considered the idealized situation of particles in a random velocity field circling around an idealized eddy. The cross-stream velocity as a function of time is modeled as the sum of a cosine function and a random component

$$u_{\perp}(n\Delta t) = r(n\Delta t)\cos(n\pi\Delta t) + u^{rand}(n\Delta t) \tag{B1}$$

$$u_{||}(n\Delta t) = r(n\Delta t)\sin(n\pi\Delta t) + u^{rand}(n\Delta t) + u_m \tag{B2}$$

where $u^{rand}(n\Delta t) = f_m \star \xi(n\Delta t)$. Here, u_m is a constant mean flow that does not play any role in the cross-stream dispersion. Random numbers ξ are generated to have a normal distribution with standard deviation σ, and then filtered with a boxcar filter f_m with m points. The variance σ^2 determines the value to which the diffusivity will converge. The filter scale m determines the time lag when the diffusivity has converged. For the particles to loop around a circle the radius r is set to r_0 for some duration t_c to $t_c + 4\pi$ to circle twice, and t_c to $t_c + \pi$ for the half circle meander, and is zero otherwise.

[53] **Acknowledgments.** This research was supported by the National Science Foundation grants OCE-0549225, OCE-9985203/OCE-0049066, and OPP-0337998 by the National Aeronautics and Space Administration contract EOS/03-0602-0117 and the Office of Science (BER), U.S. Department of Energy, grant DE-FG02-05ER64119. The global simulation was carried out as part of a Department of Defense High Performance Computing Modernization Program (HPCMP) grand challenge grant at the Maui High Performance Computing Center (MHPCC). A.G. thanks Stefan Riha for useful discussions and comments.

References

Abernathy, R., J. Marshall, E. Shuckburgh, and M. Mazloff (2009), Studies of enhanced isopycnal mixing at deep critical levels in the Southern Ocean, *J. Phys. Oceanogr.*, *40*, 170–184.

Armi, L., and H. Stommel (1983), Four views of a portion of the North Atlantic subtropical gyre, *J. Phys. Oceanogr.*, *13*, 828–857.

Bauer, S., M. S. Swenson, A. Griffa, A. J. Mariano, and K. Owens (1998), Eddy-mean flow decomposition and eddy-diffusivity estimates in the tropical Pacific Ocean: 1. Methodology, *J. Geophys. Res.*, *103*(C13), 30,855–30,871.

Berloff, P. S., and J. C. McWilliams (2002a), Material transport in oceanic gyres. Part I: Phenomenology, *J. Phys. Oceanogr.*, *32*, 764–796.

Berloff, P. S., and J. C. McWilliams (2002b), Material transport in oceanic gyres. Part II: Hierarchy of stochastic models, *J. Phys. Oceanogr.*, *32*, 797–830.

Bower, A. S., H. T. Rossby, and J. L. Lillibridge (1985), The Gulf Stream—Barrier or blender?, *J. Phys. Oceanogr.*, *15*, 24–32.

Bryden, H. L., and S. A. Cunningham (2003), How wind-forcing and air-sea heat exchange determine the meridional temperature gradient and stratification for the Antarctic Circumpolar Current, *J. Geophys. Res.*, *108*(C8), 3275, doi:10.1029/2001JC001296.

Cerovecki, I., R. A. Plumb, and W. Heres (2009), Eddy transport and mixing in a wind and buoyancy driven jet on a sphere, *J. Phys. Oceanogr.*, *39*, 1133–1149.

Danabasoglu, G., and J. Marshall (2007), Effects of vertical variations of thickness diffusivity in an ocean general circulation model, *Ocean Modell.*, *18*, 122–141.

Davis, R. (1987), Modelling eddy transport of passive tracers, *J. Mar. Res.*, *45*, 635–666.

Davis, R. (1991), Observing the general circulation with floats, *Deep Sea Res.*, *38*, suppl. 1, S531–S571.

Davis, R. (2005), Intermediate-depth circulation of the Iindian and South Pacific oceans measured by autonomous floats, *J. Phys. Oceanogr.*, *35*, 683–707.

Döös, K., and D. Webb (1994), The Deacon cell and other meridional cells of the Southern Ocean, *J. Phys. Oceanogr.*, *24*, 429–442.

Eden, C. (2006), Thickness diffusivity in the Southern Ocean, *Geophys. Res. Lett.*, *33*, L11606, doi:10.1029/2006GL026157.

Eden, C., R. J. Greatbatch, and D. Olbers (2007), Interpreting eddy fluxes, *J. Phys. Oceanogr.*, *37*(5), 1282–1296.

Efron, B., and G. Gong (1977), A leisurely look at the bootstrap, the jackknife, and cross-validation, *Am. Stat.*, *37*, 36–48.

Ferreira, D., J. Marshall, and P. Heimbach (2005), Estimating eddy stresses by fitting dynamics to observations using a residual-mean ocean circulation model and its adjoint, *J. Phys. Oceanogr.*, *35*, 1891–1910.

Freeland, H., P. Rhines, and T. Rossby (1975), Statistical observations of the trajectories of neutrally buoyant floats in the North Atlantic, *J. Mar. Res.*, *33*, 383–404.

Garaffo, Z. D., A. J. Mariano, A. Griffa, C. Veneziani, and E. P. Chassignet (2001), Lagrangian data in a high-resolution numerical simulation of the North Atlantic, *J. Mar. Syst.*, *29*, 157–176.

Gent, P. R., and J. C. McWilliams (1990), Isopycnal mixing in ocean circulation models, *J. Phys. Oceanogr.*, *20*, 150–155.

Green, J. S. (1970), Transfer properties of the large-scale eddies and the general circulation of the atmosphere, *Q. J. R. Meteorol. Soc.*, *96*, 157–185.

Griesel, A., S. T. Gille, J. Sprintall, J. L. McClean, and M. E. Maltrud (2009), Assessing eddy heat flux and its parameterization: A wavenumber perspective from a 1/10° ocean simulation, *Ocean Modell.*, *29*, 248–260, doi:10.1016/j.ocemod.2009.05.004.

Griffies, S. M. (1998), The Gent-McWilliams skew flux, *J. Phys. Oceanogr.*, *28*, 831–841.

Jayne, S. R., and J. Marotzke (2002), The oceanic eddy heat transport, *J. Phys. Oceanogr.*, *32*, 3328–3345.
Johnson, G. C., and H. L. Bryden (1989), On the size of the Antarctic Circumpolar Current, *Deep Sea Res.*, *36*, 39–53.
Kamenkovich, I., P. Berloff, and J. Pedlosky (2009), Anisotropic material transport by eddies and eddy-driven currents in a model of the North Atlantic, *J. Phys. Oceanogr.*, *39*, 3162–3175.
Keffer, T., and G. Holloway (1988), Estimating Southern Ocean eddy flux of heat and salt from satellite altimetry, *Nature*, *332*, 624–626.
Killworth, P. D. (1997), On the parameterization of eddy transfer. Part I: Theory, *J. Mar. Res.*, *55*, 1171–1197.
Krauss, W., and C. Böning (1987), Lagrangian properties of eddy fields in the northern North Atlantic as deduced from satellite-tracked buoys, *J. Mar. Res.*, *45*, 259–291.
LaCasce, J. H. (2000), Floats and f/H, *J. Mar. Res*, *58*, 61–65.
LaCasce, J. H. (2008), Lagrangian statistics from oceanic and atmospheric observations, in *Transport and Mixing in Geophysical Flows*, edited by J. B. Weiss and A. Provenzale, pp. 165–218, Springer, Berlin.
Large, W. G., J. C. McWilliams, and S. C. Doney (1994), Oceanic vertical mixing: A review and a model with a nonlocal boundary layer parameterization, *Rev. Geophys.*, *32*(4), 363–403.
Lumpkin, R., A.-M. Treguier, and K. Speer (2001), Lagrangian eddy scales in the Northern Atlantic Ocean, *J. Phys. Oceanogr.*, *32*, 2425–2440.
Maltrud, M. E., and J. L. McClean (2005), An eddy resolving global 1/10° ocean simulation, *Ocean Modell.*, *8* (1–2), 31–54.
Marshall, J., and T. Radko (2003), Residual mean solutions for the Antarctic Circumpolar Current and its associated overturning circulation, *J. Phys. Oceanogr.*, *33*(11), 2341–2354.
Marshall, J., and G. Shutts (1981), A note on rotational and divergent eddy fluxes, *J. Phys. Oceanogr.*, *11*, 1677–1680.
Marshall, J., D. Olbers, H. Ross, and D. Wolf-Gladrow (1993), Potential vorticity constraints on the dynamics and hydrography of the Southern Ocean, *J. Phys. Oceanogr.*, *23*, 456–487.
Marshall, J., E. Shuckburgh, H. Jones, and C. Hill (2006), Estimates and implications of surface eddy diffusivity in the Southern Ocean derived from tracer transport, *J. Phys. Oceanogr.*, *36*, 1806–1821.
McClean, J. L., P.-M. Poulain, J. W. Pelton, and M. L. Maltrud (2002), Eulerian and Lagrangian statistics from surface drifters and a high-resolution POP simulation in the North Aatlantic, *J. Phys. Oceanogr.*, *32*, 2472–2491.
Nakamura, N. (1996), Two-dimensional mixing, edge formation, and permeability in area coordinates, *J. Atmos. Sci.*, *53*, 1524–1537.
Oh, S. I., V. Zhurbas, and W. S. Park (2000), Estimating horizontal diffusivity in the East Sea (Sea of Japan) and the northwest Pacific from satellite-tracked drifter data, *J. Geophys. Res.*, *105*, 6483–6492.
Olbers, D., and M. Visbeck (2005), A model of the zonally averaged stratification and overturning in the Southern Ocean, *J. Phys. Oceanogr.*, *35*, 1190–1205.
Phillips, H. E., and S. R. Rintoul (2000), Eddy variability and energetics from direct current measurements in the Antarctic Circumpolar Current south of Australia, *J. Phys. Oceanogr.*, *30*, 3050–3075.
Poulain, P.-M., and P. P. Niiler (1989), Statistical analysis of the surface circulation in the California Current System using satellite-tracked drifters, *J. Phys. Oceanogr.*, *19* (10), 1588–1603.
Poulain, P.-M., A. Warn-Varnas, and P. P. Niiler (1996), Near-surface circulation of the Nordic seas as measured by Lagrangian drifters, *J. Geophys. Res.*, *101*, 18,237–18,258.
Sallée, J. B., K. Speer, R. Morrow, and R. Lumpkin (2008), An estimate of Lagrangian eddy statistics and diffusion in the mixed layer of the Southern Ocean, *J. Mar. Res.*, *66*, 441–463.
Shuckburgh, E., H. Jones, J. Marshall, and C. Hill (2009a), Robustness of effective diffusivity diagnostic in oceanic flows, *J. Phys. Oceanogr.*, *39*, 1993–2009.
Shuckburgh, E., H. Jones, J. Marshall, and C. Hill (2009b), Understanding the regional variability of eddy diffusivity in the Pacific sector of the Southern Ocean, *J. Phys. Oceanogr.*, *39*, 2011–2023.
Smith, K., and J. Marshall (2009), Evidence for deep eddy mixing in the Southern Ocean, *J. Phys. Oceanogr.*, *39*, 50–69.
Speer, K., S. R. Rintoul, and B. M. Sloyan (2000), The diabatic Deacon cell, *J. Phys. Oceanogr.*, *30*, 3212–3222.
Stammer, D. (1998), On eddy characteristics, eddy transports and mean flow properties, *J. Phys. Oceanogr.*, *28*, 727–739.
Swenson, M. S., and P. P. Niiler (1996), Statistical analysis of the surface circulation of the California Current, *J. Geophys. Res.*, *101*(C10), 22,631–22,645.
Taylor, G. I. (1921), Diffusion by continuous movements, *Proc. R. Soc. London A*, *64*, 476–490.
Treguier, A. M. (1999), Evaluating eddy mixing coefficients from eddy-resolving ocean models: A case study, *J. Mar. Res.*, *57*, 89–108.
Treguier, A. M., I. M. Held, and V. D. Larichev (1997), Parameterization of quasigeostrophic eddies in primitive equation ocean models, *J. Phys. Oceanogr.*, *27*, 567–580.
Veneziani, M., A. Griffa, A. M. Reynolds, and A. J. Mariano (2004), Oceanic turbulence and stochastic models from subsurface Lagrangian data for the north-west Atlantic Ocean, *J. Phys. Oceanogr.*, *34*, 1884–1906.
Veneziani, M., A. Griffa, Z. D. Garraffo, and E. P. Chassignet (2005a), Lagrangian spin parameter and coherent structures from trajectories released in a high-resolution ocean model, *J. Mar. Res.*, *63*, 753–788.
Veneziani, M., A. Griffa, A. M. Reynolds, Z. D. Garraffo, and E. P. Chassignet (2005b), Parameterizations of lagrangian spin statistics and particle dispersion in presence of coherent vortices, *J. Mar. Res.*, *63*, 1057–1083.
Veronis, G. (1975), The role of models in tracer studies, in *Numerical Models of Ocean Circulation*, pp. 133–146, Natl. Acad. of Sci., Washington, D. C.
Visbeck, M., J. Marshall, and T. Haine (1997), Specification of eddy transfer coefficients in coarse-resolution ocean circulation models, *J. Phys. Oceanogr.*, *27*, 381–402.
Waugh, D. W., and E. R. Abraham (2008), Stirring in the global surface ocean, *Geophys. Res. Lett.*, *35*, L20605, doi:10.1029/2008GL035526.
Zhurbas, V., and S. I. Oh (2003), Lateral diffusivity and Lagrangian scales in the Pacific Ocean as derived from drifter data, *J. Geophys. Res.*, *108* (C5), 3141, doi:10.1029/2002JC001596.
Zhurbas, V., and S. I. Oh (2004), Drifter-derived maps of lateral diffusivity in the Pacific and Atlantic oceans in relation to surface circulation patterns, *J. Geophys. Res.*, *109*, C05015, doi:10.1029/2003JC002241.

S. T. Gille, A. Griesel, J. L. McClean, and J. Sprintall, Scripps Institution of Oceanography, University of California, San Diego, 8622 Discovery Way, La Jolla, CA 92093-0230, USA. (agriesel@ucsd.edu)

J. H. LaCasce, Meteorology and Oceanography Section, Department of Geosciences, University of Oslo, PO Box 1022 Blindern, N-0315 Oslo, Norway.

M. E. Maltrud, Los Alamos National Laboratory, PO Box 1663, Los Alamos, NM 87545, USA.